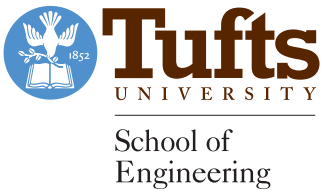

Bivelocity Hydrodynamics of Micro-Channel Couette Flow

A thesis submitted by

Peter L. L. Walls

In partial fulfillment of the requirements

for the degree of

Master of Science

in

Mechanical Engineering

TUFTS UNIVERSITY

May 2013

Advisor: Behrouz Abedian

Abstract

A nonkinetic approach is adopted in this thesis to numerically predict the profiles of a Maxwellian ideal gas in a micro-channel geometry. Our analysis utilizes a full set of mechanically and thermodynamically consistent volume-diffusion hydrodynamic equations. Bivelocity theory predicts, contrary to current investigations, a no-slip velocity at the wall in planar Couette flow for rarefied gas flows. This thesis was motivated by the recent success of Bivelocity hydrodynamics in explaining traditionally non-continuum phenomenon in a physically sound manner. The results are compared and contrasted with the Burnett equations, which show that the predictions are fundamentally different from those previously obtained in similar analyses. It is concluded that more experimental data will be needed to make a determination as to which model should be used. Suggestions for experimental verification, motivated by our numerical results, are also presented.

Acknowledgements

First and foremost, I would like to thank my advisor, Professor Behrouz Abedian, without whom this thesis would not have been possible. His open door policy and patience for my onslaught of questions has honed my thinking and helped me to grow as a researcher. I am grateful to consider him more than an advisor; he is also a good friend.

I would also like to thank Professor Howard Brenner for not only introducing me to his theory of Bivelocity hydrodynamics, but also volunteering his time to mentor me throughout this long and arduous process. I enjoyed his stories from his graduate student days; these stories will help to influence my career choices going forward. I truly cannot thank Howard enough for everything he has done for me.

In addition, I would like to thank my committee members, Professor Mark Kachanov and Professor Christoph Börgers. Our conversations were both insightful and helpful for clarifying my thesis during the editing process.

for Stephanie

my best friend and better half

Contents

1 Introduction

Microelectromechanical systems have had a major impact on our daily lives and many disciplines [1] (e.g. biology, medicine, optics, aerospace, and mechanical and electrical engineering) over the past three decades. For example hard-disk heads, micro-pumps, and lab-on-a-chip technologies all rely on gas flows around micro-scale geometry, therefore a fundamental understanding of these flows, referred to as microfluidics, is important for the design and characterization of these devices. While it is agreed that this class of gas flow is vital to many industries, there is currently no generally accepted fluid-mechanical theory for this regime of flow [2, 3]. It is this gap in knowledge that been the primary motivation of this thesis.

The critical parameter used in determining whether a particular flow is considered a continuum or non-continuum gas flow, i.e. rarefied, is the Knudsen number. The Knudsen number is typically defined as $Kn = \lambda/L$ where λ is the mean free path of the gas and L is a characteristic length scale of the geometry of interest. For example, in the case of micro-poiseuille flow L would be the diameter of the tube. The Knudsen number is commonly taken as a measure of the flows level of local equilibrium with flows possessing a higher Knudsen number being further from local thermal equilibrium. Specifically when $Kn \sim O(1)$ it is thought that there are not enough particle-to-particle collisions to equilibrate heat and momentum at every point in the flow and the local equilibrium assumption becomes increasingly inaccurate. It should also be stated that there is no objective distinction between a continuum and a non-continuum gas flow [2]. That is, there is no definite value of the Knudsen number which determines whether a gas is rarefied or otherwise. However, for the purposes of this thesis we will use the oft cited value of 0.01 to mark the transition between a continuum and a rarefied gas [4].

Prior to Knudsen's pioneering work in 1909 [5, 6] it was believed that the compressible form of the Navier-Stokes-Fourier (NSF) equations [7–9] were accurate in describing rarefied gas flows. However, Knudsen showed, through a series of experiments involving rarefied gas flows, that the compressible NSF equations, subject to the no-slip boundary condition, were inadequate in describing such flows [10]. Since this time, the rarefied or non-continuum domain of flow investigated by Knudsen is typically regarded as being governed by the Boltzmann gas-kinetic equation [1, 4, 10]. However, the mathematical complexity of the Boltzmann equation has prevented an exact solution from being derived and has lead to a variety of approximate methods being developed. These approximate solutions can be classified as either particle methods or moment methods [11]. The direct simulation Monte Carlo (DSMC) method [12,13], which will not be discussed in any depth in the body of this thesis (See Appendix C) , falls into the particle method category while the Burnett equations [10, 14] is an example of a moment method. However, the Burnett equations are known to violate a number of thermodynamic and mechanical principles (See Appendix D) [11, 15]. Despite these problems with the Burnett equations, the complexity and computational cost of DSMC and other simulation methods, such as molecular dynamics (See Appendix B), has led researchers to continue focus on the development of several different "Burnett regime" expansions of the Boltzmann equation in an attempt to fix these violations and accurately capture the physics of the problem while reducing computational complexity. "Burnett regime" simply refers to the agreed upon range of $0.01 < Kn_0 < 10$ also referred to as the transition regime. These expansions are referred to as: Burnett equations [14], conventional Burnett equations [10], augmented Burnett equations [16], and the BKG-Burnett equations [17], each of which has attempted to resolve issues with the original Burnett equations. To this day

however, in the field of rarefied gas flow there does not exist an uncontested, generally applicable, macroscopic fluid-mechanical theory [2, 3].

Recently Bivelocity hydrodynamics [18–21], a new theory proposed by Howard Brenner has attempted to close the gap of understanding in rarefied gas flows. To date this new theory has been successful in describing experimental data in both continuum and non-continuum fluid flows [22–24]. These experiments range from thermophoresis [25, 26] to describing the enhanced mass flow rate of micro-channel pressure driven flows [23]. Bivelocity theory's hypothesis, that there exist two independent velocities in any compressible fluid, differs substantially from the traditional approach for describing not only rarefied gases but compressible flows in general. While Bivelocity hydrodynamics has been applied to several non-continuum experiments with great success, the theory was originally derived using the macroscopic non-kinetic framework of Linear Irreversible Thermodynamics [9] (LIT) and in the past couple of years has been verified using a kinetic-theory approach [15, 27, 28]. Given the success of bivelocity hydrodynamics in describing a variety of both compressible and micro-channel flows in a physically sound manner, we have investigated the predictions this new theory gives for micro-Couette, the simple shear driven flow between two infinite parallel plates.

2 Bivelocity Hydrodynamics Overview

2.1 Generic Transport Equations

2.1.1 Eulerian Transport

In this section an overview will be given of the generic transport equations, in order to highlight the theoretical development of the Bivelocity hydrodynamic

equations [19, 21]. Beginning with any extensive physical property Ψ we can write an equation representing the total amount of this quantity in an arbitrary volume. The quantity Ψ can represent any physical quantity such as mass M, momentum $\boldsymbol{M}$, internal energy U, entropy S, etcetera. The amount Ψ at time t at a fixed point in space $\boldsymbol{x}$ ($\boldsymbol{x}$ here representing an arbitrary position vector) encompassed in a volume V can be given by:

$$\Psi(t) = \int_V \psi(\boldsymbol{x}, t)\, dV \tag{2.1}$$

where $\psi(\boldsymbol{x}, t)$ is the amount of the physical property per unit volume. We can now determine the total change of this property over time by taking the temporal derivative to (2.1) yield:

$$\frac{d\Psi}{dt} = \int_V \frac{\partial}{\partial t}\left[\psi(\boldsymbol{x}, t)\right] dV \tag{2.2}$$

This total change of the property can be attributed to two physical mechanisms: a flux through the surrounding surface of the volume; and production of the quantity within the arbitrary volume. The surface flux mechanism can be expressed generally in terms of a total flux density $\boldsymbol{n}_\psi(\boldsymbol{x}, t)$ as follows:

$$-\oint_S \hat{\boldsymbol{n}} \cdot \boldsymbol{n}_\psi(\boldsymbol{x}, t)\, dS \tag{2.3}$$

with $\hat{\boldsymbol{n}}$ and dS representing the outward facing surface normal vector and differential scalar surface quantities, respectively. Next, the total production of the property in the volume can be given in terms of a per unit volume production term $\pi_\psi(\boldsymbol{x}, t)$ as:

$$\int_V \pi_\psi(\boldsymbol{x}, t)\, dV \tag{2.4}$$

Now, with the use of the divergence theorem to transform (2.3) into the proper volume based form below:

$$-\oint_S \hat{\boldsymbol{n}} \cdot \boldsymbol{n}_\psi \left(\boldsymbol{x}, t\right) dS = -\int_V \nabla \cdot \boldsymbol{n}_\psi \left(\boldsymbol{x}, t\right) dV \tag{2.5}$$

Through combining (2.2), (2.4) and (2.5) for an arbitrary volume, the total generic Eulerian transport equation becomes:

$$\frac{\partial \psi}{\partial t} + \nabla \cdot \boldsymbol{n}_\psi = \pi_\psi \tag{2.6}$$

and represents the unsteady transport of any extensive physical property when given in terms of ψ, i.e. amount of property per unit volume. The first and most recognizable use for the Eulerian form of the transport equation is to denote the transport of mass M. For this case our per unit volume mass is simply the density ρ and since mass is a conserved quantity, i.e. $\pi_m = 0$, the result is the well known continuity equation:

$$\frac{\partial \rho}{\partial t} + \nabla \cdot \boldsymbol{n}_m = 0 \tag{2.7}$$

wherein when the density flux is represented in terms of the local mass velocity, i.e. $\mathbf{n}_m = \rho \mathbf{v}_m$, the standard form of the continuity equation is furnished:

$$\frac{\partial \rho}{\partial t} + \nabla \cdot (\rho \boldsymbol{v}_m) = 0 \tag{2.8}$$

2.1.2 Diffusive Molecular Flux

As is traditionally done [8], before continuing to the other transport equations, we will break the total Eulerian flux $\boldsymbol{n}_\psi$ into two physically distinct components: a convective contribution and a molecular or diffusive contribution as follows:

$$\boldsymbol{n}_\psi := \boldsymbol{n}_m\hat{\psi} + \boldsymbol{j}_\psi \tag{2.9}$$

The convective portion of the total flux $\boldsymbol{n}_m\hat{\psi}$ is given in terms of the mass flux $\boldsymbol{n}_m$ and the property specific density $\hat{\psi} = \psi/\rho$, which represents the amount of the physical property per unit mass that is carried along with the mass flux across the bounding surface. The other contribution, i.e. the diffusive molecular flux $\boldsymbol{j}_\psi$, represents the amount of the property per unit time flowing non-convectively across a unit area. This allows us to define the diffuse molecular flux as the difference between the total Eulerian flux $\boldsymbol{n}_\psi$ and the convective contribution $\boldsymbol{n}_m\hat{\psi}$:

$$\boldsymbol{j}_\psi := \boldsymbol{n}_\psi - \boldsymbol{n}_m\hat{\psi} \tag{2.10}$$

The diffusive molecular flux $\boldsymbol{j}_\psi$, which going forward will be referred to as simply the diffuse flux, is not directly measured in experiment [21]. However, this diffuse flux is defined in terms of three separately measureable fields and should be considered a slack variable to represent the difference observed. Note, that when the property being transported is mass i.e. $\hat{\psi} = 1$, the diffuse flux is identical to zero and corresponds with the definition of no mass being diffusively transported.

2.1.3 Lagrangian Transport Equations

Before presenting the remaining transport equations, we will want to transform the generic Eulerian equation (2.7) into the more familiar Lagrangian form (2.11). This transformation is equivalent to changing our perspective from focusing on a single point in the flow (Eulerian) to following a packet of fluid as it moves with the flow (Lagrangian). By combining the continuity equation

(2.7) and the definition of the diffuse molecular flux (2.9) we can yield:

$$\rho \frac{D\hat{\psi}}{Dt} + \nabla \cdot \boldsymbol{j}_{\psi} = \pi_{\psi} \tag{2.11}$$

with the material derivative defined as:

$$\frac{D}{Dt} := \frac{\partial}{\partial t} + \boldsymbol{v}_m \cdot \nabla \tag{2.12}$$

We now have the general Lagrangian form that we will be utilizing throughout the remainder of this thesis.

Contextual Velocities

Before moving on and presenting the derivation of the specific equations constituting Bivelocity hydrodynamics, we would like to give a high level overview of the theory and how it differs from the traditional Navier-Stokes-Fourier approach.

Since Euler's founding of the subject of ideal fluid mechanics [29], the "contextual" velocities defined by their appearances in the body force free mass (2.13), momentum (2.14), and energy (2.15) equations have been implicitly assumed equal to the mass velocity present in the continuity equation (2.13).

$$\frac{\partial \rho}{\partial t} + \nabla \cdot (\rho \boldsymbol{v}_m) = 0 \tag{2.13}$$

$$\rho \frac{D\hat{\boldsymbol{m}}}{Dt} + \nabla \cdot \boldsymbol{P} = 0 \tag{2.14}$$

$$\rho \frac{D}{Dt} \left(\hat{u} + \frac{1}{2} |\boldsymbol{v}_{kin}|^2 \right) + \nabla \cdot (\boldsymbol{j}_u + \boldsymbol{P} \cdot \boldsymbol{v}_v) = 0 \tag{2.15}$$

If we name each velocity according to their corresponding location in the above equations the resulting terminology is:

$$\boldsymbol{v}_m := Mass\ Velocity$$

$$\hat{\boldsymbol{m}} := Momentum\ Velocity$$

$$\boldsymbol{v}_{kin} := Kinetic\ Velocity$$

$$\boldsymbol{v}_v := Volume\ Velocity$$

Moving forward, if we are to assume any equality between the above named "contextual" velocities, it must be proven. However, Landau and Lifshitz in 1959 [7] were the first to recognize the need to prove one of the implicit assumptions, namely the Euler hypothesis ($\hat{\boldsymbol{m}} = \boldsymbol{v}_m$), rather than accept it as a fact based on an analogy to Newtonian mechanics. Kostddt and Liu [30] later recognized their proof as incomplete and offered a more convincing argument in favor of Euler's hypothesis. Liu drawing upon thermodynamic and mechanical arguments [31], further elaborated upon his proof. This proof by Liu was endorsed by Öttinger [32] and led to a collaboration with Liu and Struchtrup, which stated that rejection of Euler's hypothesis would lead to, among other things, violation of the principle of locally conserved angular momentum [33] and therefore the two velocities ($\hat{\boldsymbol{m}}, \boldsymbol{v}_m$) must at all times be equal. It is interesting to note that the complete proof of this equality wasn't published until 2009!

Lastly, the equality ($\hat{\boldsymbol{m}} = \boldsymbol{v}_{kin}$) is shown [34] to be necessary to satisfy the required physical principle of Galilean invariance (recognized as an indisputable universally valid physical principle) of the mass, momentum, and energy equations. We now have proofs stating that ($\hat{\boldsymbol{m}} = \boldsymbol{v}_{kin} = \boldsymbol{v}_m$) for all fluids, however, no such proof has been given stating the equality of $\boldsymbol{v}_v$ to any of the

other velocities. It is this lack of evidence for the equality of $\boldsymbol{v}_v$ that is the essence of the Bivelocity hydrodynamics paradigm.

2.2 Pre-Constitutive Bivelocity Transport Equations

In what follows we will present the pre-constitutive transport equations governing Bivelocity hydrodynamics for volume, energy, and momentum. By pre-constitutive it is meant the following transport equations do not provide enough information to fully describe the physical problem and will require several constitutive hypotheses for closure. These constitutive hypotheses, as will be seen in Section 2.3, are material dependent and will be derived using the principles of LIT.

The transport of mass is excluded in this section due to the resulting equation, when written in Lagrangian form, equalling $0 = 0$, which provides no useful information.

2.2.1 Volume Transport

Volume is a generally non-conserved property in any given system, i.e. $\pi_\nu \neq 0$. To illustrate this point, if one takes a quantity of hot water and mixes it both adiabatically and isobarically with a quantity of cold water; once this mixture is allowed to equilibrate to a temperature between the two components the resulting volume will, in general, be different than just the sum of the two individual quantities [35]. That is to say that water doesn't follow a rule of thermal additive volumes.

Now applying the general Lagrangian transport equation (2.11) with $\hat{\psi} = \hat{v} = 1/\rho$ we can write the transport of volume as:

$$\rho \frac{D\hat{v}}{Dt} + \nabla \cdot \boldsymbol{j}_v = \pi_v \tag{2.16}$$

with $\hat{v}$ representing the fluid's specific volume and $\boldsymbol{j}_v$ representing the diffuse volume flux. We can write the volume transport (2.16) in the Eulerian form (2.6) with $\psi = 1$ which results in:

$$\nabla \cdot \boldsymbol{n}_\nu = \pi_\nu \tag{2.17}$$

and can be seen as a sort of "volumetric continuity equation" [35]. Volume production π_v is philosophically different from the other transport quantities in that there is no counterpart for π_v in discrete Newtonian mechanics [21]. This owes to the fact that each point size particle constituting a continuum contains no volume and at best this property can be attributed to a collection of particles in a statistical manner. The point-size particles, on the other hand, do carry the properties of mass, momentum, and energy rendering them fundamentally different.

2.2.2 Momentum Transport

The production of momentum given in Bivelocity theory is not changed from that of the production given in the NSF case and is defined as:

$$\pi_{\boldsymbol{M}} = -\nabla p + \rho \hat{\boldsymbol{f}} \tag{2.18}$$

with p being the equilibrium thermodynamic pressure and $\hat{\boldsymbol{f}}$ a conservative specific body force, such as gravity, that derives from a time-independent potential, i.e. $\left(\partial\hat{\phi}/\partial t = 0\right)$:

$$\hat{\boldsymbol{f}} = -\nabla\hat{\phi} \tag{2.19}$$

The Lagrangian transport equation (2.11), along with the fluids per unit volume momentum being $\boldsymbol{M} = \boldsymbol{v}_m\rho$, becomes:

$$\rho\frac{D\boldsymbol{v}_m}{Dt} + \nabla\cdot\boldsymbol{j_M} = -\nabla p + \rho\hat{\boldsymbol{f}} \tag{2.20}$$

wherein $\boldsymbol{j_M}$ is the diffuse flux of momentum and is defined in terms of the pressure tensor $\boldsymbol{P}$ and equilibrium pressure p:

$$\boldsymbol{j_M} := \boldsymbol{P} - \boldsymbol{I}p \tag{2.21}$$

2.2.3 Energy Transport

The production term in the Bivelocity energy equation is changed from that of the original NSF equations from the concept of mechanical work $\nabla\cdot(\boldsymbol{P}\cdot\boldsymbol{v}_m)$ to that of irreversible thermodynamic work:

$$\pi_e = -\nabla\cdot(\boldsymbol{P}\cdot\boldsymbol{v}_v) \tag{2.22}$$

with the pressure tensor $\boldsymbol{P}$. The volume velocity $\boldsymbol{v}_v$, also referred to as the "work velocity" is defined solely by its assigned role in (2.22) [21]. An excellent discussion comparing and contrasting the concepts of the traditional mechanical work with the newly introduced irreversible thermodynamic work is presented in [34, Section X]. Also note that while the mass velocity $\boldsymbol{v}_m$ does not require a constitutive equation, the volume velocity $\boldsymbol{v}_v$ appearing in (2.22) does require a constitutive hypothesis. Now using the Lagrangian transport equation (2.11) we arrive at:

$$\rho\frac{D\hat{e}}{Dt} + \nabla\cdot\boldsymbol{j}_u = -\nabla\cdot(\boldsymbol{P}\cdot\boldsymbol{v}_v) \tag{2.23}$$

wherein

$$\hat{e} = \hat{u} + \hat{e}_k + \hat{\phi} \tag{2.24}$$

is the fluid's specific energy, consisting of the internal, kinetic, and potential energies. The specific kinetic energy is given by the classical relation $\hat{e}_k = (1/2)\,\boldsymbol{v}_m \cdot \boldsymbol{v}_m$. Above we have written the energy equation in terms of the diffuse flux of internal energy by setting $\boldsymbol{j}_e = \boldsymbol{j}_u$. This is true by definition since there can be no diffuse flux of either kinetic or potential energy (for single-component fluids, which for this thesis is our focus)

2.3 Constitutive Equations

In the prior section we presented a complete set of pre-constitutive equations, but still require constitutive equations for the pressure tensor $\boldsymbol{P}$, the diffuse flux of internal energy $\boldsymbol{j}_u$, and the volume velocity $\boldsymbol{v}_v$ to complete closure. Note that we chose to exclude the entropy transport equation in the prior section as we will not be utilizing it in this thesis.

We will now discuss how the general principles of linear irreversible thermodynamics (i.e. non-equilibrium thermodynamics) [9] were used in the derivation of the constitutive relationships for $(\boldsymbol{v}_v, \boldsymbol{P}, \boldsymbol{j}_u)$. The full derivation has been presented in a comprehensive review of Bivelocity theory to date [21] and will not be presented here. We will simply be presenting the results along with illustrating some of the important features of the theory.

2.3.1 Volume Velocity

The relation between the mass velocity $\boldsymbol{v}_m$ and the volume velocity $\boldsymbol{v}_v$ is connected through the concept of a diffuse volume flux as follows [21, 36]:

$$\boldsymbol{v}_v = \boldsymbol{v}_m + \boldsymbol{j}_v \tag{2.25}$$

with $\boldsymbol{j}_v$ being the diffuse flux of volume. This diffuse flux requires a constitutive

equation, and is given by [21]:

$$\boldsymbol{j}_v = \alpha \nabla \ln \rho - \alpha \kappa \rho \hat{\boldsymbol{f}} \tag{2.26}$$

In this expression α and κ represent the fluids thermometric diffusivity and compressibility coefficient. This same relationship between the volume and mass velocity along with the constitutive equation for the volume flux has been derived by Dadzie [15] and independently by Eu [36–39] from purely kinetic-theory standpoints, which has given the theory a firm grounding in the kinetic theory field. Both of these derivations showed that when volume transport is added to the molecular transport equation (e.g. the Boltzmann equation), the relationships (2.25) and (2.26) naturally arise from the governing equation.

2.3.2 Pressure Tensor

For an ideal gas, i.e. a fluid in which we can ignore bulk viscosity effects, we can express the pressure tensor in the standard form

$$\boldsymbol{P} = \boldsymbol{I}p - \boldsymbol{T} \tag{2.27}$$

where p is the equilibrium thermodynamic pressure and $\boldsymbol{T}$ is the viscous or deviatoric stress tensor. Also, we will restrict the viscous stress tensor to being both symmetric and traceless, i.e. $\overline{\boldsymbol{D}} = \frac{1}{2}\left(\boldsymbol{D} + \boldsymbol{D}^T\right) - \frac{1}{3} tr\left(\boldsymbol{D}\right)$ where the superscript ^{T} is the transpose and $tr\left(\ \right)$ is the trace of the tensor. Now, the stress tensor is given in terms of the volume velocity as follows:

$$\boldsymbol{T} = 2\mu \overline{\nabla \boldsymbol{v}_v} \tag{2.28}$$

which is in stark contrast to the NSF case, given in terms of the mass velocity

$$\boldsymbol{T} = 2\mu\overline{\nabla \boldsymbol{v}_m} \tag{2.29}$$

Also note that when $\boldsymbol{j}_v = 0$, as is the case for incompressible flow, the stress tensor (2.28) assumes the form of (2.29).

2.3.3 Diffuse Flux of Internal Energy

The last constitutive relation required for the closure of the transport equations is the diffuse flux of internal energy. In Bivelocity hydrodynamics the flux of internal energy $\boldsymbol{j}_u$ is linked to the traditional heat flux $\boldsymbol{q}$ as follows:

$$\boldsymbol{j}_u = \boldsymbol{q} - p\boldsymbol{j}_v \tag{2.30}$$

with the only remaining unknown requiring a constitutive relation being that of the entropic or traditional heat flux. In conventional NSF fluid mechanics, which is equivalent to $\boldsymbol{j}_v = 0$, the fluxes are identical, as should be expected. The entropic heat flux is now given as:

$$\boldsymbol{q} = -kT\nabla \ln T + \alpha\beta T\left(\nabla p - \rho\hat{\boldsymbol{f}}\right) \tag{2.31}$$

with k and β representing the fluids thermal conductivity and thermal expansivity.

We now have all of the transport equations with their respective constitutive hypotheses that are required to describe the general flow of a fluid. Before applying these equations to the problem of micro-Couette flow we much first address the boundary conditions.

3 No-slip Boundary Condition

The plane micro-Couette flow analysed in this thesis is a unique class of fluid flow. Steady micro-Couette flow is different from other cases in that there are no gradients in the direction of flow. For instance, in other flows there may be either a pressure or temperature gradient along the direction of fluid flow. This difference will be seen to make a substantial difference in our predictions for the appropriate boundary conditions for micro-Couette flow.

Traditionally for micro-channel flow, where the Knudsen number can be of $O(1)$, a slip-velocity would be imposed at the boundaries. This slip velocity, originally given by Maxwell [40], is given as a function of either the first or second orders of the velocity gradient as follows:

$$(u_m)_{slip} \propto \left.\frac{\partial u}{\partial n}\right|_{wall} \tag{3.1}$$

and is related to the shear stress at the bounding wall. However, in keeping with the boundary condition proposed by Brenner [21, 34, 41], we will instead use a no-slip on the volume velocity condition, shown below:

$$(\boldsymbol{I} - \hat{\boldsymbol{n}}\hat{\boldsymbol{n}}) \cdot \boldsymbol{v}_v = 0 \tag{3.2}$$

in which $\boldsymbol{I}$ is the idiom factor and $\hat{\boldsymbol{n}}$ is the unit surface normal vector. Given the definitions of the volume velocity $\boldsymbol{v}_v$ (2.25) and diffuse volume flux $\boldsymbol{j}_v$ (2.26), it can prove useful to express this boundary condition as a slip on the mass velocity:

$$(\boldsymbol{v}_m)_{slip} = -\alpha \left.\frac{\partial \ln \rho}{\partial s}\right|_{wall} \tag{3.3}$$

where ∂s refers to the differential distance measured along the wall in which

the slip or creep occurs and α is the fluid's thermal diffusivity.

We will take the position originally adopted by Stokes [42, 43] regarding determining the accuracy of theory [41]. That is to say that the viability of the volume-velocity boundary condition can only be made certain by examining the pertinent experimental evidence. To date the slip condition (3.2), (3.3) above has been successfully applied to both the phenomena of thermophoresis [22] and predicting the enhanced mass flow rates of pressure-driven rarefied gases [23, 44–47]. Thermophoresis, for example, was previously explained by a sub-continuum thermal creep boundary condition which relied upon free parameters, the degree of scattering for a particle hitting a surface for example, to fit the experimental data [34, 48]. However, an analysis utilizing Bivelocity hydrodynamics [22] resulted in a first-principles prediction that fit experimental data well, and was also free of any empirical fitting parameters. This success of fitting the experimental data, along with the lack of any convincing experimental evidence for the existence of a slip-velocity in plane Couette flow, gives us confidence that application of the condition above results in the most consistent and accurate analysis of the flow in this geometry.

4 Plane Micro-Couette Flow

Steady flow between infinite parallel plates is a simple geometry for feasible testing of micro-channel models. This model provides insights into analogous systems such as gas bearings and disc-head readers. The geometry in this thesis will consist of a fixed lower plate separated ($y = 0$) by a small distance H from an upper plate moving at a constant velocity V and can be seen in Figure 1 below.

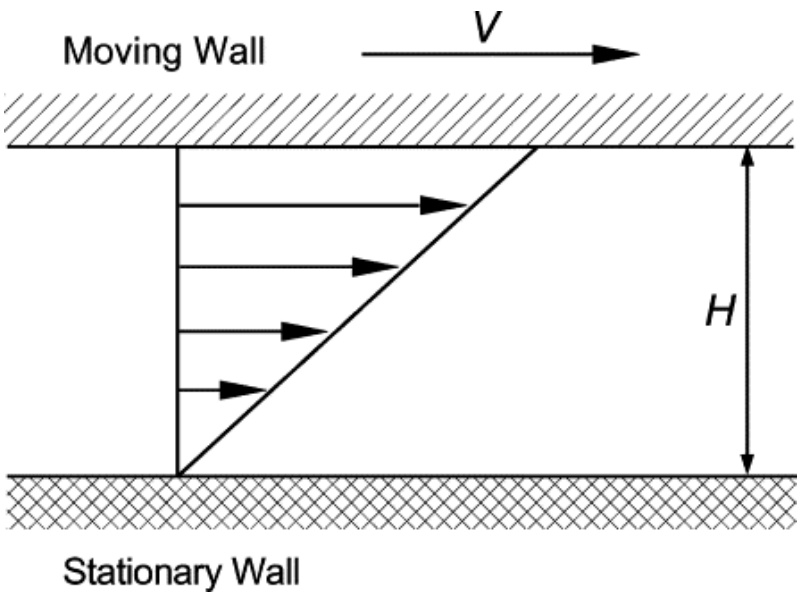

Figure 1: Micro-Couette flow geometry [49]

For the steady flow we are considering, given the lack of experimental data in this flow regime, it will prove useful to compare and contrast the predictions given by Bivelocity hydrodynamics with those of the conventional Burnett model. Beginning with the transport equations of Burnett, for this steady Couette flow, they reduce to the following set of ordinary differential equations [10, 49, 50]:

$$\frac{d}{dy}\left[\mu\frac{du}{dy}\right] = 0 \tag{4.1}$$

$$\frac{d}{dy}\left[p + \mathbf{\Pi}_{22}^{(2)}\right] = 0 \tag{4.2}$$

$$\frac{d}{dy}\left[k\frac{dT}{dy} + \mu u\frac{du}{dy}\right] = 0 \tag{4.3}$$

with k representing the gas's thermal conductivity, p the equilibrium thermodynamic pressure, and μ the dynamic viscosity. Going forward we will represent the mass velocity in the x-direction by u. The variable $\mathbf{\Pi}_{22}^{(2)}$ here represents a second-order contribution to the stress tensor and is given as:

$$\mathbf{\Pi}_{22}^{(2)} = \frac{\mu^2}{p}\left[\alpha_1\left[\frac{du}{dy}\right]^2 + \alpha_2 R\frac{d^2T}{dy^2} + \alpha_3\frac{RT}{\rho}\frac{d^2\rho}{dy^2} + \alpha_4\frac{RT}{\rho^2}\left[\frac{d\rho}{dy}\right]^2 + \alpha_5\frac{R}{\rho}\frac{d\rho}{dy}\frac{dT}{dy} + \alpha_6\frac{R}{T}\left[\frac{dT}{dy}\right]^2\right] \tag{4.4}$$

Where α_{1-6} are constant coefficients given during the derivation as:

$$\alpha_1 = -\frac{2}{3},\ \alpha_2 = \frac{2}{3},\ \alpha_3 = -\frac{4}{3},\ \alpha_4 = \frac{4}{3},\ \alpha_5 = -\frac{4}{3},\ \alpha_6 = 2$$

The above set of equations (4.1), (4.2), and (4.3) with the higher-order contribution $\mathbf{\Pi}_{22}^{(2)}$ (4.4) constitute a complete set of non-linear ordinary differential equations and in conjunction with an appropriate equation of state (4.8) can be solved numerically with appropriate boundary conditions.

Now, as with the Burnett equations above, we will present the reduced versions of the Bivelocity equations for comparison

$$\frac{d}{dy}\left[\mu\frac{du}{dy}\right] = 0 \tag{4.5}$$

$$\frac{d}{dy}\left[p - \frac{4}{3}\mu\frac{dj_v}{dy}\right] = 0 \tag{4.6}$$

$$\frac{d}{dy}\left[k\frac{dT}{dy} + \mu u\frac{du}{dy} - \frac{k}{\rho\hat{c}_p}\frac{dp}{dy} + \frac{4}{3}\mu j_v\frac{dj_v}{dy}\right] = 0 \tag{4.7}$$

From (4.6) and (4.7) we can immediately see the role of the diffuse volume flux j_v in both the momentum and energy equations. This stands in stark contrast to the Burnett equations which only have a "higher-order" contribution to the momentum equation (4.2). One also notices that all three equations given by Bivelocity theory are coupled together, in that all three differential equations

must be solved simultaneously. However, it can be seen that the Burnett equations (4.1) and (4.3) depend only upon the temperature and mass velocity and are solved independently of equation (4.2). This "decoupled" nature makes solving the Burnett equations more straightforward and allows us to simply use the results for the velocity and temperature fields in determining the density.

We now have both sets of differential equations and only require an appropriate equation of state. In this thesis the fluid being analysed is assumed to be a Maxwellian monatomic ideal gas, where Maxwellian is referring to the intermolecular potential. This assumption will greatly simplify the differential equations and their subsequent solutions along with allowing us to easily incorporate the effects of temperature on the transport properties. The state of a monatomic ideal gas flow can be fully characterized by its density ρ, temperature T, and mass velocity u. We also assume that the gas is in a state of local equilibrium to enable use of the ideal gas law

$$p = \rho RT \tag{4.8}$$

wherein R is the specific gas constant. While we recognize that for flows approaching a Knudsen number on the order of unity the local equilibrium assumption breaks down, since the Knudsen number itself can be seen as a measure of local equilibrium, we will still use the ideal gas law as an approximation, as is traditionally done [49, 50]. For a monatomic gas the isochoric and isobaric specific heats $\hat{c}_v$ and $\hat{c}_p$ are related to the specific gas constant by the relations

$$\hat{c}_v = \frac{3}{2}R \text{ and } \hat{c}_p = \frac{5}{2}R$$

such that the specific heat ratio γ which is defined as $\hat{c}_p/\hat{c}_v = 5/3$. The speed

of sound in the gas is given by the simple relation as

$$c^2 = \gamma \frac{p}{\rho} \tag{4.9}$$

Lastly, for a Maxwellian monatomic gas modelled by point centres of force, the thermal conductivity and dynamic viscosity are directly proportional to temperature [49–51], i.e. $(\mu, k) \propto T$, and will be used to incorporate the effect of temperature on these properties in our analysis. For convenience in calculations we will non-dimensionalize the flow variables and properties as follows, in a manner similar to Xue [50]:

$$\tilde{y} = \frac{y}{H},\ \tilde{u} = \frac{u}{\sqrt{RT_0}},\ \tilde{T} = \frac{T}{T_0},\ \tilde{\rho} = \frac{\rho}{\rho_0},\ \tilde{p} = \frac{p}{p_0},\ \tilde{\mu} = \frac{\mu}{\mu_0},\ \tilde{k} = \frac{k}{\mu_0 \hat{c}_p}$$

where the subscript "0" indicates the value of the property or variable at the stationary wall ($y = 0$). The constant Prandtl number for a monatomic gas $\mathrm{Pr} = \mu\hat{c}_p/k = 2/3$ is used in the following relations for the dimensionless viscosity and thermal conductivity to incorporate the effects of temperature into the model.

$$\tilde{\mu} = \tilde{T} \text{ and } \tilde{k} = \frac{3}{2}\tilde{T}$$

The Knudsen and Mach numbers are defined as

$$Kn_0 = \frac{\mu_0}{\rho_0 \sqrt{RT_0} H} \tag{4.10}$$

and

$$Ma = \frac{V}{c_0}$$

where the reduced Knudsen number (4.10) given above can be related to the commonly used definition of the Knudsen number

$$Kn = \frac{\lambda}{H}$$

as $Kn_0 = 0.783Kn$ owing to the definition of the mean free path of the reference state for an ideal gas [52]

$$\lambda = \frac{16}{5\sqrt{2\pi}} \frac{\mu_0}{\rho_0 \sqrt{RT_0}}$$

Using the above defined dimensionless parameters we will re-write the Burnett equations (4.1), (4.2), and (4.3) along with the higher order stress term (4.4) as

$$\frac{d}{d\tilde{y}} \left[\tilde{T} \frac{d\tilde{u}}{d\tilde{y}} \right] = 0 \tag{4.11}$$

$$\frac{d}{d\tilde{y}} \left[\tilde{p} + {Kn_0}^2 \tilde{\mathbf{\Pi}}^{(\mathbf{2})}_{\mathbf{22}} \right] = 0 \tag{4.12}$$

$$\frac{d}{d\tilde{y}} \left[\frac{15}{4} \tilde{T} \frac{d\tilde{T}}{d\tilde{y}} + \tilde{T}\tilde{u} \frac{d\tilde{u}}{d\tilde{y}} \right] = 0 \tag{4.13}$$

with $\tilde{\mathbf{\Pi}}^{(\mathbf{2})}_{\mathbf{22}}$ equalling

$$\begin{aligned} \tilde{\mathbf{\Pi}}^{(\mathbf{2})}_{\mathbf{22}} = \frac{\tilde{T}^2}{\tilde{p}} \Bigg[\alpha_1 \left[\frac{d\tilde{u}}{d\tilde{y}} \right]^2 + \alpha_2 \frac{d^2\tilde{T}}{d\tilde{y}^2} + \alpha_3 \frac{\tilde{T}}{\tilde{\rho}} \frac{d^2\tilde{\rho}}{d\tilde{y}^2} \\ + \alpha_4 \frac{\tilde{T}}{\tilde{\rho}^2} \left[\frac{d\tilde{\rho}}{d\tilde{y}} \right]^2 + \alpha_5 \frac{1}{\tilde{\rho}} \frac{d\tilde{\rho}}{d\tilde{y}} \frac{d\tilde{T}}{d\tilde{y}} + \alpha_6 \frac{1}{\tilde{T}} \left[\frac{d\tilde{T}}{d\tilde{y}} \right]^2 \Bigg] \end{aligned} \tag{4.14}$$

Now, nondimensionalization of the Bivelocity equations (4.5), (4.6), and (4.7)

results in

$$\frac{d}{d\tilde{y}}\left[\tilde{T}\frac{d\tilde{u}}{d\tilde{y}}\right] = 0 \tag{4.15}$$

$$\frac{d}{d\tilde{y}}\left[\tilde{p} - \frac{4}{3}Kn_0{}^2\tilde{T}\frac{d\tilde{j}_v}{d\tilde{y}}\right] = 0 \tag{4.16}$$

$$\frac{d}{d\tilde{y}}\left[\frac{15}{4}\tilde{T}\frac{d\tilde{T}}{d\tilde{y}} + \tilde{T}\tilde{u}\frac{d\tilde{u}}{d\tilde{y}} - \frac{3}{2}\frac{\tilde{T}}{\tilde{\rho}}\frac{d\tilde{p}}{d\tilde{y}} + \frac{4}{3}Kn_0{}^2\tilde{T}\tilde{j}_v\frac{d\tilde{j}_v}{d\tilde{y}}\right] = 0 \tag{4.17}$$

wherein we have introduced the dimensionless diffuse volume flux

$$\tilde{j}_v = \frac{3}{2}\frac{\tilde{T}}{\tilde{\rho}^2}\frac{d\tilde{\rho}}{d\tilde{y}}$$

Both sets of differential equations will be subject to the following dimensionless boundary conditions:

Fixed Bottom Plate ($\tilde{y} = 0$):

$$\tilde{\rho} = 1,\ \tilde{T} = 1,\ \tilde{u} = 0$$

Moving Top Plate ($\tilde{y} = 1$):

$$\tilde{\rho} = 1,\ \tilde{T} = 1,\ \tilde{u} = \gamma^{0.5}Ma$$

Upon inspection of (4.12), (4.16), and (4.17) we can see that these equations are of third order in terms of the density and second order in temperature and velocity. Also, we note that there are no Knudsen number effects on either the temperature or velocity distributions. The solution to the Burnett equations, regardless of how rarefied the gas is, will always coincide with the standard NSF solution (the so called Brinkman solution), since the higher order terms

only affect the density profile as is seen by inspection of (4.2). The Bivelocity equations, on the other hand, will be seen to be affected by the order of the Knudsen number. In order to reduce the total order from seven to six and facilitate applying boundary conditions we will use the method of Lee [52], which was adopted and implemented by both Xue [50] and Lockerby [49] in their studies of the Burnett equations. Using this method will also allow us to directly compare and contrast our results with both Lockerby and Xue. The method is straightforward and relies on the assumption that after integrating the y-direction momentum equations (4.12) and (4.16) once to reduce their order, the resulting constant is independent of the Knudsen number. Integrating both equations once results in:

$$\tilde{p} + {Kn_0}^2 \tilde{\mathbf{\Pi}}^{(\mathbf{2})}_{\mathbf{22}} = \tilde{K}_1 \tag{4.18}$$

and

$$\tilde{p} - \frac{4}{3} {Kn_0}^2 \tilde{T} \frac{d\tilde{j}_v}{d\tilde{y}} = \tilde{K}_2 \tag{4.19}$$

In the limit $Kn_0 \to 0$ the dimensionless pressure gradient disappears identically in both (4.12) and (4.16), which corresponds to the traditional NSF case of constant pressure across the channel. This assumption allows us to assign the values of $\tilde{K}_1 = 1$ and $\tilde{K}_2 = 1$ and continue our analysis by reducing the total order of our non-linear system of ODE's to six. Using (4.18) the reduced order equations corresponding to the Burnett equations (4.11), (4.12), and (4.13), with some rearrangement and combining of terms, are:

$$\tilde{T} \frac{d^2\tilde{u}}{d\tilde{y}^2} + \frac{d\tilde{T}}{d\tilde{y}} \frac{d\tilde{u}}{d\tilde{y}} = 0 \tag{4.20}$$

$$\frac{\tilde{T}}{\tilde{\rho}}\frac{d^2\tilde{\rho}}{d\tilde{y}^2} - \frac{19}{30}\left[\frac{d\tilde{u}}{d\tilde{y}}\right]^2 - \frac{1}{\tilde{T}}\left[\frac{d\tilde{T}}{d\tilde{y}}\right]^2 - \frac{\tilde{T}}{\tilde{\rho}^2}\left[\frac{d\tilde{\rho}}{d\tilde{y}}\right]^2 + \frac{1}{\tilde{\rho}}\frac{d\tilde{\rho}}{d\tilde{y}}\frac{d\tilde{T}}{d\tilde{y}} + \frac{3}{4}\frac{\tilde{\rho}}{\tilde{T}}\frac{1-\tilde{\rho}\tilde{T}}{{Kn_0}^2} = 0 \tag{4.21}$$

$$\tilde{T}\frac{d^2\tilde{T}}{d\tilde{y}^2} + \left[\frac{d\tilde{T}}{d\tilde{y}}\right]^2 + \frac{4}{15}\tilde{T}\left[\frac{d\tilde{u}}{d\tilde{y}}\right]^2 = 0 \tag{4.22}$$

Now, if we perform similar operations on (4.15), (4.16), and (4.17) instead using (4.19) to reduce the order of the Bivelocity equations (see Appendix A for more details) we arrive at:

$$\tilde{T}\frac{d^2\tilde{u}}{d\tilde{y}^2} + \frac{d\tilde{T}}{d\tilde{y}}\frac{d\tilde{u}}{d\tilde{y}} = 0 \tag{4.23}$$

$$\tilde{T}\frac{d^2\tilde{\rho}}{d\tilde{y}^2} + \frac{d\tilde{T}}{d\tilde{y}}\frac{d\tilde{\rho}}{d\tilde{y}} - 2\frac{\tilde{T}}{\tilde{\rho}}\left[\frac{d\tilde{\rho}}{d\tilde{y}}\right]^2 + \frac{1}{2}\frac{\tilde{\rho}^2}{\tilde{T}}\frac{1-\tilde{\rho}\tilde{T}}{{Kn_0}^2} = 0 \tag{4.24}$$

$$\tilde{T}\frac{d^2\tilde{T}}{d\tilde{y}^2} + \left[\frac{d\tilde{T}}{d\tilde{y}}\right]^2 + \frac{4}{9}\tilde{T}\left[\frac{d\tilde{u}}{d\tilde{y}}\right]^2 + \frac{1}{3}\frac{1}{\tilde{T}}\frac{1-\tilde{\rho}\tilde{T}}{{Kn_0}^2} = 0 \tag{4.25}$$

We now have both sets of equations in a form that will facilitate a numerical solution.

4.1 Numerical Solutions

To solve the set of nonlinear differential equations both for the Burnett and Bivelocity equations we utilized the bvp4c solver in MATLAB. The bvp4c solver is a general boundary value problem solver that uses a collocation method to converge to a solution [53]. A collocation method is simply a method which chooses a higher order polynomial, for example a cubic spline, to represent the

differential equations, which matches both the boundary conditions (collocates) and the midpoint within the problem domain. The solver then chooses the solution through iteration that best matches this polynomial, i.e. has the smallest residuals. The bvp4c method can be described as a fourth order solver that solves linearized equations with an adaptive mesh. As with any boundary value problem the initial guess structure is very important and can affect the solution greatly. In order to facilitate consistent and accurate results we use the Knudsen number equal to zero case as our guess to the more general case for Knudsen numbers on of the order of unity.

4.1.1 Solver Accuracy

When using a numerical method to solve a set of equations the accuracy of the chosen method must be considered. For this study I ensured the accuracy of the solution in two ways, the values of the solution residuals were kept below 10^{-5}; and the solutions mesh independence was analyzed. The residuals, i.e. the difference between the numerical solution and the exact ODEs, is an option that can be set in bvp4c solver. The equations being solved were approximately parabolic in behavior and low residuals were always attained in the analysis. For a solution to exhibit mesh independence there must be minimal and ideally no change in the solution when a different resolution (domain divisions) is chosen. The solutions to the Burnett (4.20), (4.21) and (4.22) and Bivelocity (4.23), (4.24) and (4.25) equations resulting from applying the bvp4c method were determined to be independent of the mesh. The governing equations were first solved with 50 divisions and subsequently solved with finer meshs (100, 200, etc) until 1600 mesh points were used. During each trial there was no significant difference between the results, therefore the solutions were found to be mesh independent. Based on these criteria the numerical method was

determined to be accurate for this set of equations.

4.1.2 Initial Guess for Solver $Kn_0 \to 0$

We will take the Knudsen number equal to zero in order to form our initial guess and the resulting equations are listed below:

$$\frac{d}{d\tilde{y}}\left[\tilde{\mu}\frac{d\tilde{u}}{d\tilde{y}}\right] = 0 \tag{4.26}$$

$$\frac{d\tilde{p}}{d\tilde{y}} = 0 \tag{4.27}$$

$$\frac{d}{d\tilde{y}}\left[-\tilde{k}\frac{5}{2}\frac{d\tilde{T}}{d\tilde{y}} - \tilde{\mu}\tilde{u}\frac{d\tilde{u}}{d\tilde{y}}\right] = 0 \tag{4.28}$$

which are identical to the Navier-Stokes-Fourier equations. Both the Burnett and Bivelocity equations reduce to this form in the $Kn_0 \to 0$ case. While our velocity profile will not be strictly linear in the full model, since the fluid properties depend upon the temperature, we will assume that for the initial profile the velocity is, to a good approximation, linear and given by the profile below:

$$u = V\frac{y}{H} \tag{4.29}$$

With the non-dimensional form being

$$\tilde{u} = \gamma^{1/2} Ma \tilde{y} \tag{4.30}$$

Substituting (4.30) into (4.28) and integrating once we arrive at

$$\frac{d\tilde{T}}{d\tilde{y}} = -\frac{2}{5}\gamma\frac{\tilde{\mu}}{\tilde{k}}Ma^2\tilde{y} + \tilde{C}_1 \tag{4.31}$$

Now recognizing that

$$\mathrm{Pr} = \frac{\tilde{\mu}}{\tilde{k}} = \frac{2}{3} \tag{4.32}$$

And integrating once more

$$\tilde{T} = -\frac{4}{30}\gamma Ma^2\tilde{y}^2 + \tilde{C}_1\tilde{y} + \tilde{C}_2 \tag{4.33}$$

Now we can apply the equal temperature boundary conditions for the upper and lower plates, along with substituting $\gamma = 5/3$ for a monatomic gas, which results in:

$$\tilde{T} = 1 + \frac{2}{9}Ma^2\tilde{y}\,(1-\tilde{y}) \tag{4.34}$$

and is readily seen to be equal to the classic Brinkman solution for simple viscous shear with equal temperature boundaries. This will now be our initial profile for numerically solving the full $O\,(1)$ Knudsen number Bivelocity equations.

4.1.3 General Knudsen Number Case

We now have everything we need in order to numerically solve the full set of momentum and energy equations. Using the bvp4c solver method, we were able to obtain stable numerical solutions for a variety of Mach numbers and Knudsen numbers. We have chosen to plot the case when $Ma = 3$; other Mach numbers showed the same behaviour in the profiles just with a more or less pronounced result depending on the magnitude of the Mach number. We began with numerically solving the Burnett equations (4.20), (4.21), and (4.22) to allow for direct comparisons of our results with those of Lockerby [49] and to also ensure that our solution method is producing accurate results. Below in Figures 2 & 3 we have plotted the dimensionless density, temperature, and

velocity profiles for the Burnett equations.

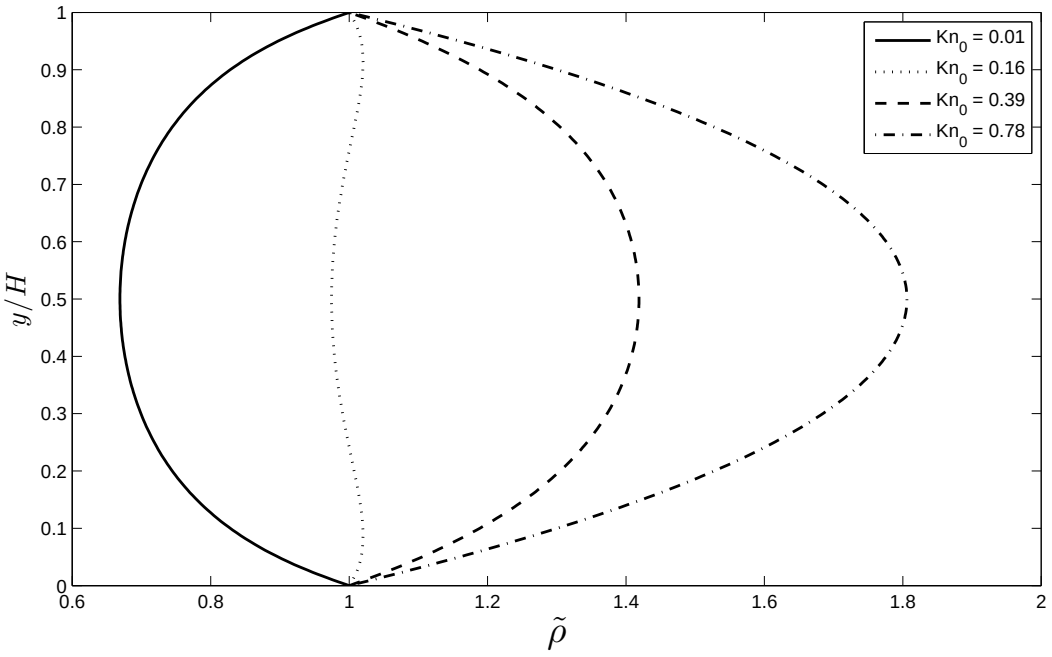

Figure 2: Burnett Density distributions across the micro-channel for $Ma = 3$, $Kn_0 = 0.01, 0.16, 0.39, 0.78$

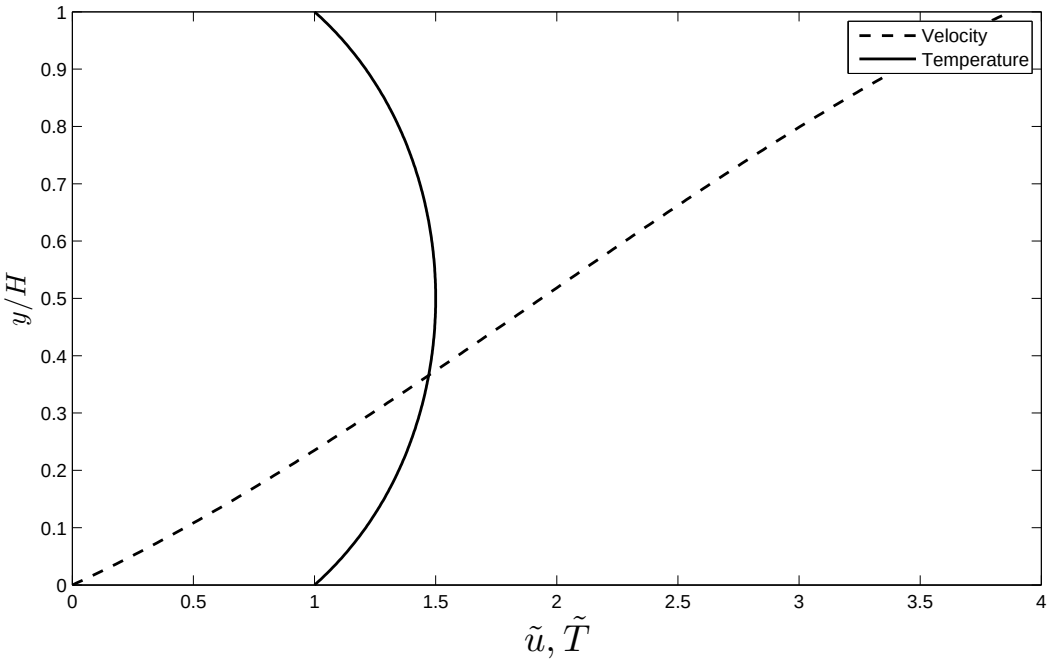

Figure 3: Burnett Velocity and temperature distributions across the micro-channel for $Ma = 3$, $Kn_0 = 0.01, 0.16, 0.39, 0.78$

Comparing the above figure with that presented in Lockerby [49], the plot matches identically when the data in Figure 2 is multiplied by 5/3 to account for the difference in non-dimensional density definitions. Next, comparing the calculated temperature and velocity profiles in Figure 3 we see that again, when the temperature is multiplied by 3/2 to account for the different definitions, the data matches that of Lockerby exactly. Since there is no dependence on the Knudsen number for either the temperature or velocity only one case is plotted.

Owing to both sets of profiles matching those given by [49], we are confident in our solution method and were able to numerically solve the Bivelocity equations (4.23), (4.24), and (4.25). Below we have presented the dimensionless density (Figure 4), along with the temperature and velocity profiles predicted by Bivelocity hydrodynamics (Figure 5). In Figure 5, while the velocity profile will vary based on the Knudsen number, we did not plot more than a single case since there was a negligible variation between the different values of Knudsen number.

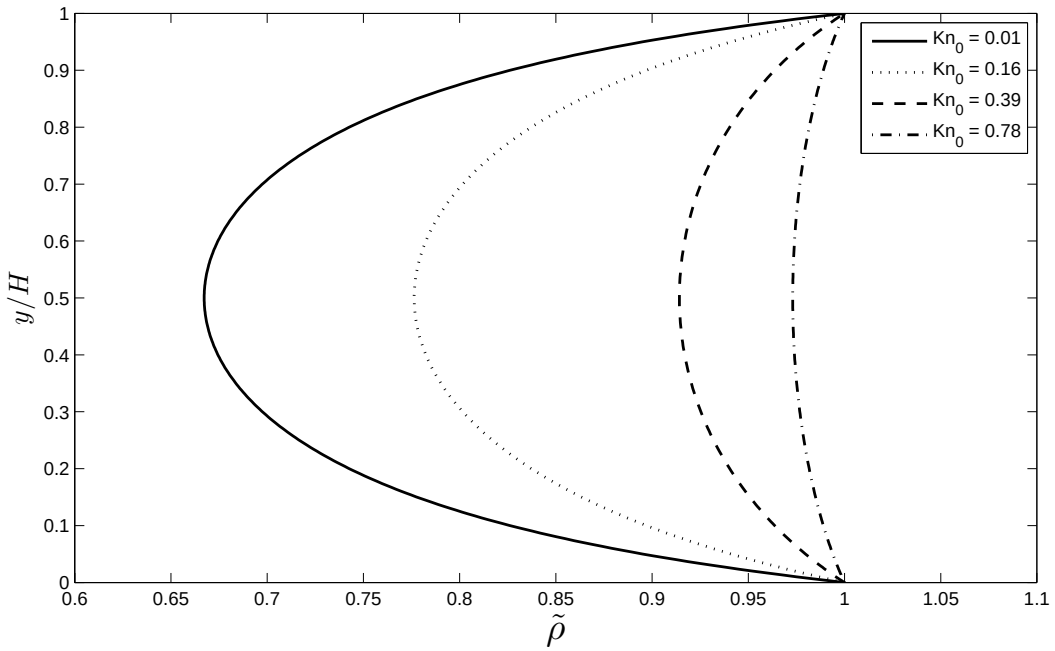

Figure 4: Bivelocity Density distributions across the micro-channel for $Ma = 3$, $Kn_0 = 0.01, 0.16, 0.39, 0.78$

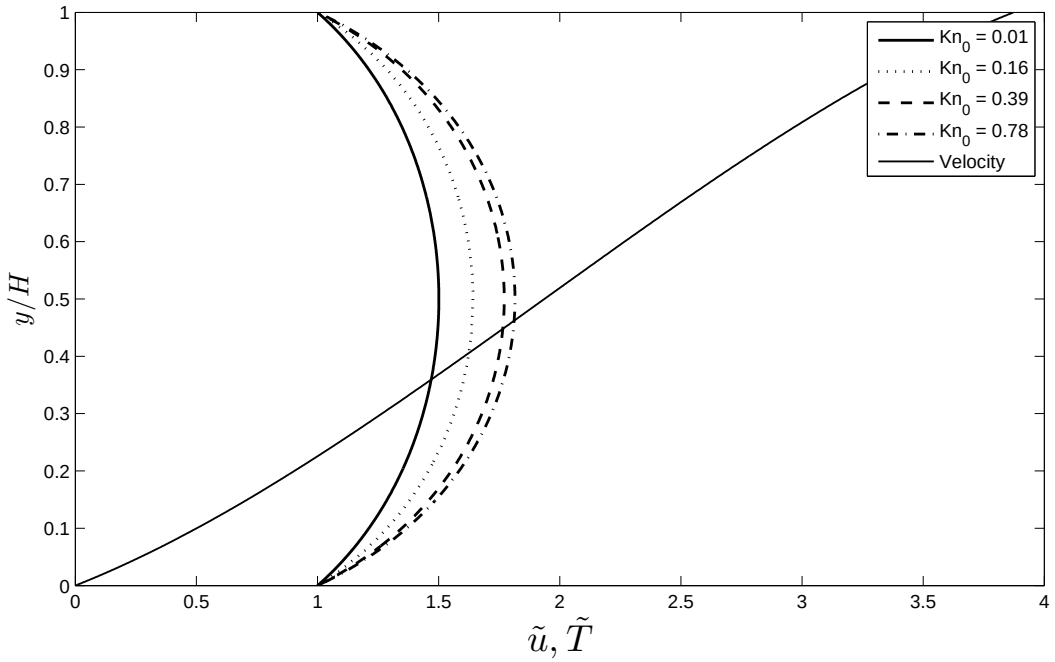

Figure 5: Bivelocity Velocity and temperature distributions across the micro-channel for $Ma = 3$, $Kn_0 = 0.01, 0.16, 0.39, 0.78$

When the results are compared with the traditional Burnett equations [49, 50] a few fundamental differences arise. First, as we mentioned earlier, the

temperature across the channel is now dependent on the value of the Knudsen number and increases as the Knudsen number increases. Secondly, while the density does increase as the Knudsen number increases in a similar manner to the Burnett solutions, there is no longer a transition period, approximately $Kn_0 \approx 0.13 - 0.23$, where the density gradient changes sign several times as was seen in the Burnett equations (see Figures 2 & 6).

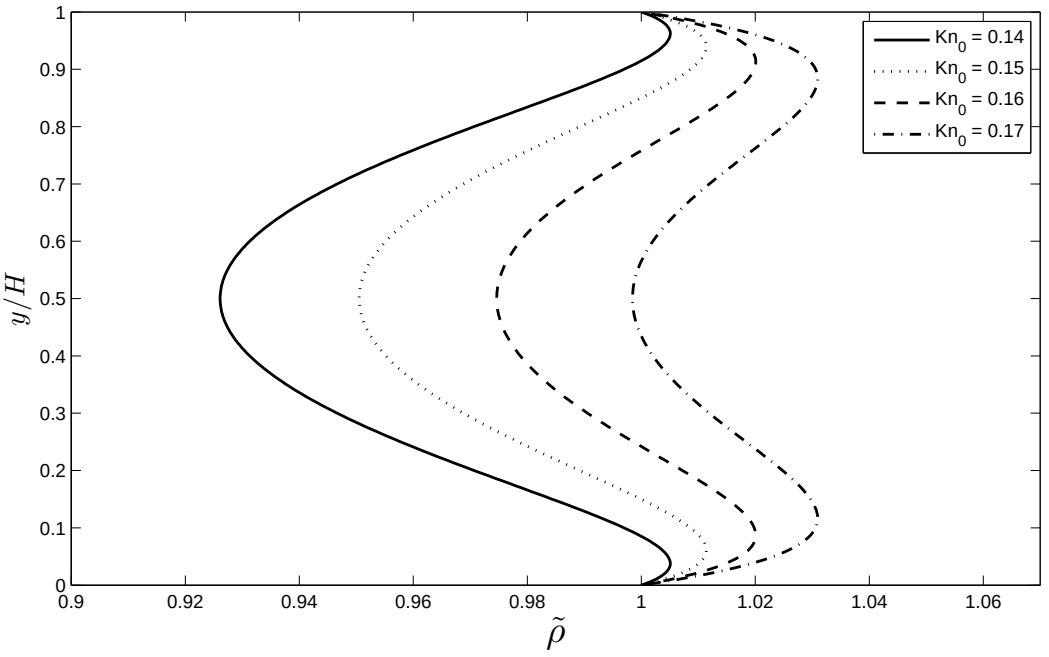

Figure 6: Transition period for density with Burnett equations $Ma = 3$, $Kn_0 = 0.01, 0.16, 0.39, 0.78$

This behaviour is not observed in the Bivelocity equations and the density approaches a maximum value equal to the boundary value as the Knudsen number increases (See Figure 4). To further illustrate this difference we examined the mass flow rate, using the following relation plotted at various Knudsen numbers.

$$\tilde{m}_{dot} = \int_{\tilde{y}=0}^{\tilde{y}=1} \tilde{u}\left(\tilde{y}\right)\tilde{\rho}\left(\tilde{y}\right) d\tilde{y} \tag{4.35}$$

where $\tilde{m}_{dot}$ is the dimensionless mass flow rate per unit depth D and is defined as

$$\tilde{m}_{dot} = \frac{m_{dot}}{D}\frac{1}{\rho_0\sqrt{RT_0}H} = \frac{Kn_0}{\mu_0}\frac{m_{dot}}{D} \tag{4.36}$$

The total mass flow rate for the Burnett case is seen to be significantly higher than that predicted with the Bivelocity equations and at $Kn_0 = 1$ the ratio is approximately

$$\frac{(\tilde{m}_{dot})_{Burnett}}{(\tilde{m}_{dot})_{Bivelocity}} \approx 1.63$$

and can be seen in Figure 7 below.

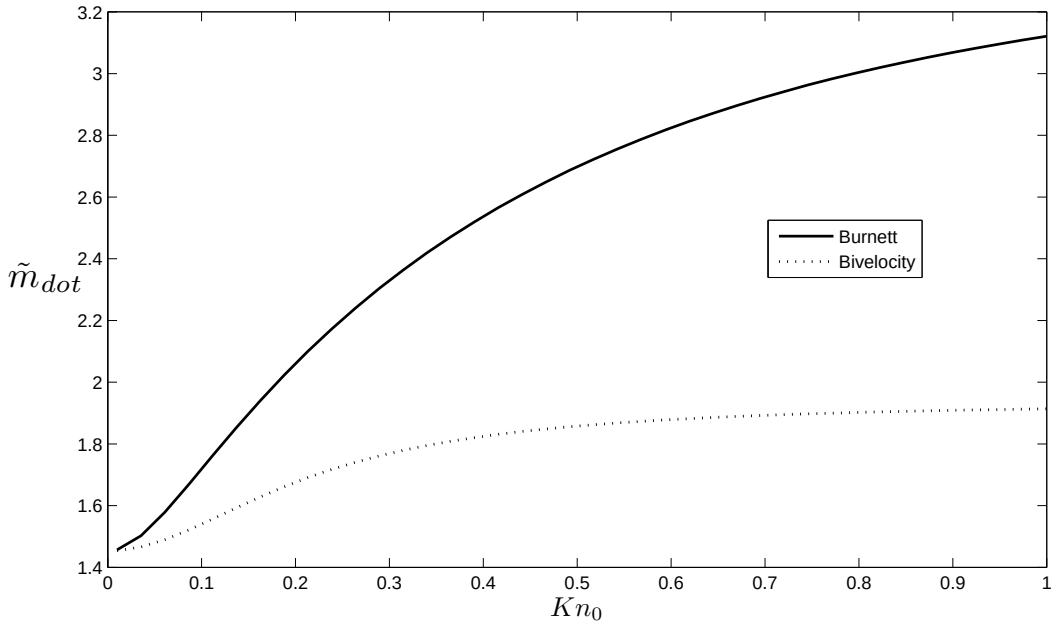

Figure 7: Dimensionless mass flow rate across the micro-channel at $Ma = 3$, $Kn_0 = 0.01 \rightarrow 1.0$

Another important physical prediction of the Bivelocity equations that differs from that of the Burnett equations is the non-zero value of the diffuse volume flux, i.e. the non-zero velocity perpendicular to the mass velocity (See Figure 8 below).

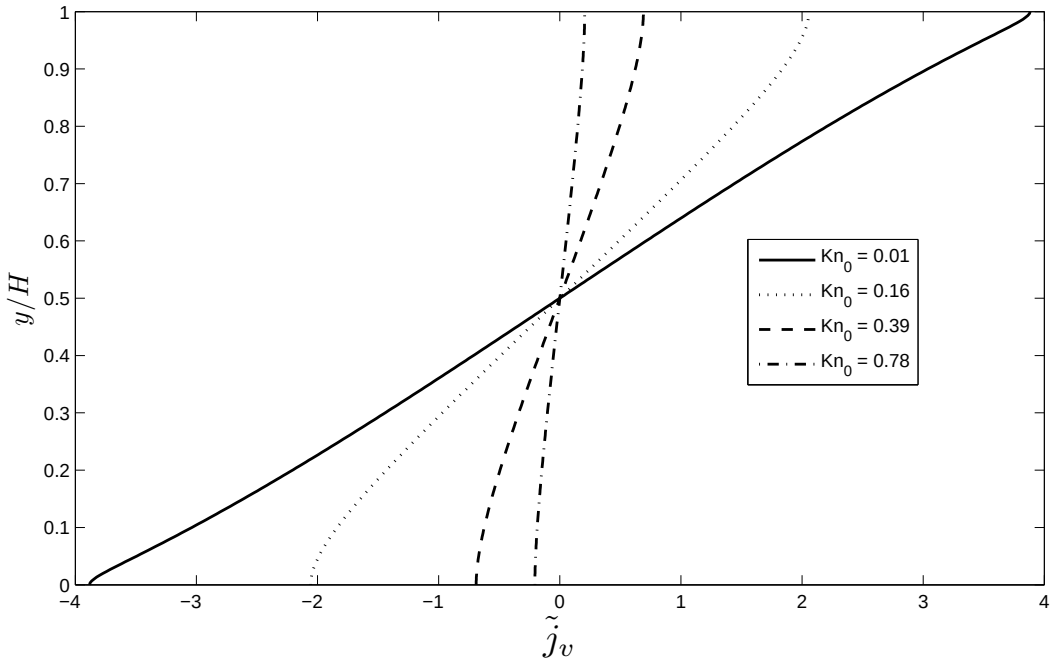

Figure 8: Bivelocity Dimensionless volume flux across the micro-channel at $Ma = 3$, $Kn_0 = 0.01, 0.16, 0.39, 0.78$

This result can be interpreted in exactly the same manner as the phenomenon of thermophoresis [22, 25]. A buoyantly neutral non-brownian particle when introduced into the channel would move towards either the bottom or top of the channel. If the particle is introduced at exactly the center of the channel it will remain there, however if the particle is introduced above the centerline ($\tilde{y} > 0.5$) it will move towards the top plate and *vice versa*, for example by examining Figure 8 one can see that all values for $\tilde{j}_v$ above the centerline are positive and will push the particle towards the moving plate.

The pressure distribution in the channel predicted by both the Burnett and Bivelocity equations differs from the constant pressure solution of the Navier-Stokes-Fourier equations. In both theories a cross channel pressure increase is predicted; this can be seen in Figures 9 & 10 below. When we consider the definition of the dimensionless pressure ($\tilde{p} = \tilde{\rho}\tilde{T}$) this result is not surprising in that both theories predict a cross-channel density increase

along with either the temperature remaining constant (Burnett) or increasing (Bivelocity). This non-constant pressure will also affect a particle being introduced into the channel. The pressure gradient would assist the thermophoretic motion and drive the particle away from the centerline towards either bounding wall. We can see from Figures 9 & 10 that the cross-channel pressure increases predicted by Bivelocity theory are nearly half that of the Burnett predictions.

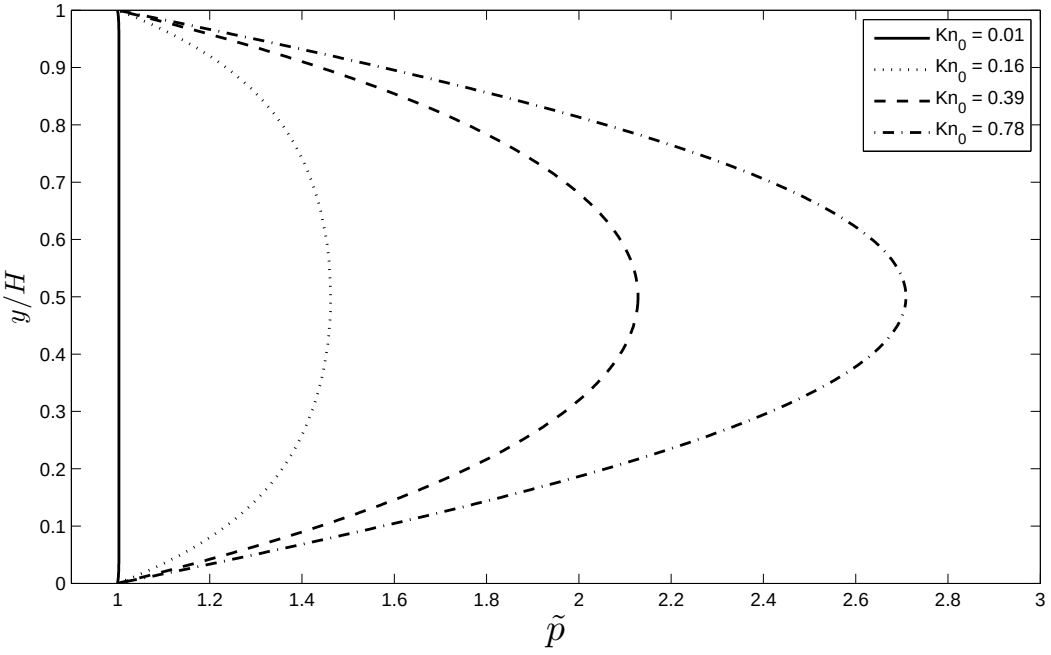

Figure 9: Burnett Dimensionless pressure distribution across the micro-channel at $Ma = 3$, $Kn_0 = 0.01, 0.16, 0.39, 0.78$

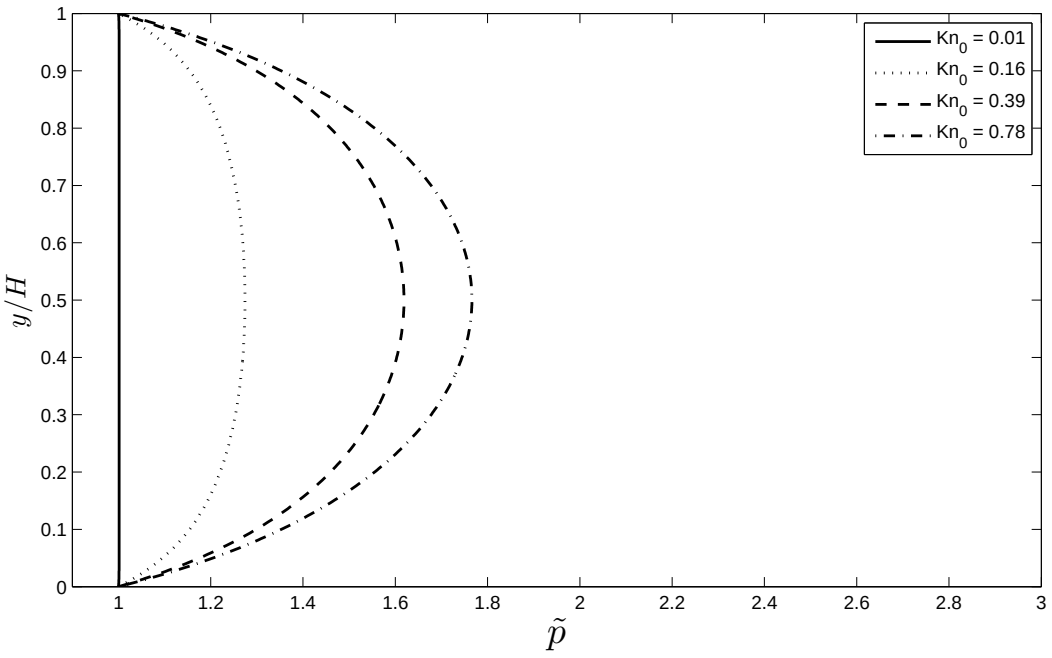

Figure 10: Bivelocity Dimensionless pressure distribution across the micro-channel at $Ma = 3$, $Kn_0 = 0.01, 0.16, 0.39, 0.78$

5 Discussion

5.1 Experimental Validation

This thesis has presented the predictions of two competing theories, Burnett and Bivelocity, to describe the behavior of a rarefied gas undergoing simple shearing. While the complete profiles for the temperature, density, and pressure have been presented; a conclusion with regards to which theory is valid cannot be made without conclusive experimental data. Currently, experimental data for this flow geometry for rarefied gases is lacking and new experiments will need to be performed in order to settle the debate.

When an experiment is inevitably performed, it will become necessary to determine the quantities of importance. For example, while directly measuring the cross channel distributions of $\tilde{T}$, $\tilde{\rho}$, or $\tilde{p}$ would allow one to determine the

accuracy of the proposed theories, the scale of this experiment would make this difficult to achieve. However, measuring the mass flow rate (4.35) would be a more straightforward method and has been successfully performed for other micro channel flow geometries. For example, in [23] Dadzie demonstrated the accuracy of Bivelocity theory, subject to the no-slip velocity on the volume velocity v_v, by comparing mass flow rate data for a micro channel pressure driven flow to the analytical predictions of Bivelocity hydrodynamics. Another benefit of comparing the mass flow rates is the degree in which the Burnett and Bivelocity solutions differ. As is seen in Figure 7, when the Knudsen number is on the order of unity, the mass flow rate of the Burnett equations is nearly double that of the Bivelocity equations and should be the focus of an experimental study.

5.2 Heat Transfer

The temperature distributions predicted by the Burnett (Figure 3) and Bivelocity (Figure 5) equations indicate their respective heat transfers will be fundamentally different. On the one hand, the Burnett equations state that the heat transfer is unaffected by the extent of gas rarefaction, while the Bivelocity equations show the converse. According to Bivelocity theory the flux of internal energy, which will be referred to as the heat flux, is given by (2.30) and (2.31). Combining these two equations, along with using the ideal gas equation, the heat flux $\mathbf{j}_u$ can be given in terms of the temperature gradient only:

$$\mathbf{j}_u = -k' \nabla T \tag{5.1}$$

where $k' = k/\gamma$. This relationship (5.1), along with the results presented in Figure 5, show that the heat flux or internal energy flux will increase as the gas

becomes increasingly rarefied. However, note that the heat flux will initially be less than the predicted value when using Fourier's law , i.e. $-k\nabla T$, owing to $1/\gamma$ equaling 3/5. This finding will also require experimental investigation and could be a good candidate to determine the accuracy of Bivelocity hydrodynamics for this geometry.

6 Conclusions

Bivelocity hydrodynamics, along with the newly introduced no-slip on the volume velocity, has been recently successful in describing experimental phenomena previously explained only through the use of ad-hoc boundary conditions, i.e. those requiring fitting parameters [22, 23]. In this analysis we have presented a full set of mechanically and thermodynamically consistent equations for steady micro-channel Couette flow. The results of which differ significantly from those given by the traditional Burnett equations. It has been shown that the magnitude of the Knudsen number not only affects the density distribution, but the temperature as well, which will also affect the internal energy flux. This thesis has shown that in this geometry a slip-velocity boundary condition is inappropriate and should be replaced with a no-slip on the volume velocity, which also corresponds to a no-slip mass velocity. Therefore in order to determine which of the competing models accurately describes this geometry, experimental data will be needed to make the more informed decision. It is concluded that an investigation of the mass flow rate in this micro-channel would be the best means to determine the accuracy of this theory's predictions.

Appendix A Reducing the order of the Bivelocity Equations

In this section we would like to give a more detailed, step-by-step, description of reducing the order (4.15), (4.16), and (4.17) to (4.23), (4.24), and (4.25) using (4.19) because it is not immediately transparent. Starting with the following

$$\frac{d}{d\tilde{y}}\left[\tilde{T}\frac{d\tilde{u}}{d\tilde{y}}\right] = 0 \tag{A.1}$$

$$\tilde{p} - \frac{4}{3}Kn_0{}^2\tilde{T}\frac{d\tilde{j}_v}{d\tilde{y}} = 1 \tag{A.2}$$

$$\frac{d}{d\tilde{y}}\left[\frac{15}{4}\tilde{T}\frac{d\tilde{T}}{d\tilde{y}} + \tilde{T}\tilde{u}\frac{d\tilde{u}}{d\tilde{y}} - \frac{3}{2}\frac{\tilde{T}}{\tilde{\rho}}\frac{d\tilde{p}}{d\tilde{y}} + \frac{4}{3}Kn_0{}^2\tilde{T}\tilde{j}_v\frac{d\tilde{j}_v}{d\tilde{y}}\right] = 0 \tag{A.3}$$

$$\tilde{j}_v = \frac{3}{2}\frac{\tilde{T}}{\tilde{\rho}^2}\frac{d\tilde{\rho}}{d\tilde{y}} \tag{A.4}$$

First, expanding the third term in (5.3) in terms of density and temperature we get

$$-\frac{3}{2}\frac{\tilde{T}}{\tilde{\rho}}\frac{d\tilde{p}}{d\tilde{y}} = -\frac{3}{2}\frac{\tilde{T}^2}{\tilde{\rho}}\frac{d\tilde{\rho}}{d\tilde{y}} - \frac{3}{2}\tilde{T}\frac{d\tilde{T}}{d\tilde{y}} \tag{A.5}$$

Next, we rearrange (A.2) in order to match the last term in (A.3) as follows

$$\left[\tilde{\rho}\tilde{T} - 1\right]\tilde{j}_v = \frac{4}{3}Kn_0{}^2\tilde{T}\tilde{j}_v\frac{d\tilde{j}_v}{d\tilde{y}} \tag{A.6}$$

Now, we recognize that the first term on the RHS of (A.5) can be rewritten in terms of the diffuse volume flux as follows

$$-\frac{3}{2}\frac{\tilde{T}}{\tilde{\rho}}\frac{d\tilde{p}}{d\tilde{y}} = -\tilde{\rho}\tilde{T}\tilde{j}_v - \frac{3}{2}\tilde{T}\frac{d\tilde{T}}{d\tilde{y}} \tag{A.7}$$

Substituting (A.6) and (A.7) into (A.3) with collecting like terms becomes

$$\frac{d}{d\tilde{y}}\left[\frac{9}{4}\tilde{T}\frac{d\tilde{T}}{d\tilde{y}} + \tilde{T}\tilde{u}\frac{d\tilde{u}}{d\tilde{y}} - \tilde{j}_v\right] = 0 \tag{A.8}$$

Now, expanding (A.8) out where we have used (A.1) to simplify the derivative of the second term in (A.8)

$$\frac{9}{4}\tilde{T}\frac{d^2\tilde{T}}{d\tilde{y}^2} + \frac{9}{4}\left[\frac{d\tilde{T}}{d\tilde{y}}\right]^2 + \tilde{T}\left[\frac{d\tilde{u}}{d\tilde{y}}\right]^2 - \frac{d\tilde{j}_v}{d\tilde{y}} = 0 \tag{A.9}$$

The last step for the energy equation is to substitute the value of $d\tilde{j}_v/d\tilde{y}$ from (A.2)

$$\tilde{T}\frac{d^2\tilde{T}}{d\tilde{y}^2} + \left[\frac{d\tilde{T}}{d\tilde{y}}\right]^2 + \frac{4}{9}\tilde{T}\left[\frac{d\tilde{u}}{d\tilde{y}}\right]^2 + \frac{1}{3}\frac{1-\tilde{\rho}\tilde{T}}{Kn_0{}^2\tilde{T}} = 0 \tag{A.10}$$

The expansion of (A.2) is more straightforward and is as follows starting with expanding $d\tilde{j}_v/d\tilde{y}$ out

$$\frac{d\tilde{j}_v}{d\tilde{y}} = \frac{3}{2}\frac{d}{d\tilde{y}}\left[\frac{\tilde{T}}{\tilde{\rho}^2}\frac{d\tilde{\rho}}{d\tilde{y}}\right] = \frac{3}{2}\frac{\tilde{T}}{\tilde{\rho}^2}\frac{d^2\tilde{\rho}}{d\tilde{y}^2} + \frac{3}{2}\frac{1}{\tilde{\rho}^2}\frac{d\tilde{T}}{d\tilde{y}}\frac{d\tilde{\rho}}{d\tilde{y}} - 3\frac{\tilde{T}}{\tilde{\rho}^3}\left[\frac{d\tilde{\rho}}{d\tilde{y}}\right]^2 \tag{A.11}$$

Now substituting this into (A.2) and rearranging we acquire our last equation

$$\tilde{T}\frac{d^2\tilde{\rho}}{d\tilde{y}^2} + \frac{d\tilde{T}}{d\tilde{y}}\frac{d\tilde{\rho}}{d\tilde{y}} - 2\frac{\tilde{T}}{\tilde{\rho}}\left[\frac{d\tilde{\rho}}{d\tilde{y}}\right]^2 + \frac{1}{2}\frac{\tilde{\rho}^2}{\tilde{T}}\frac{1-\tilde{\rho}\tilde{T}}{Kn_0{}^2} = 0 \tag{A.12}$$

Appendix B Molecular Dynamics

Molecular dynamics (MD) is essentially a computer simulation which tracks all of the individual atoms along with their velocities and momentums in the volume of interest. While it is true that real systems are governed by the principles of quantum mechanics, it would be impractical to solve the full many-body problem [54]. MD simulations are therefore governed by the laws of classical mechanics, most notably Newton's second law $\mathbf{F}_i = m_i\mathbf{a}_i$. Each atom i in a system composed of N atoms carries with it information regarding its coordinates and momentum, which gives the "dynamical state" of a many-body system [55].

Now, any thermo or hydrodynamic state variable that depends on these quantities can be derived from local spatial or time averages. This technique, i.e. that utilizing Newton's second law, is considered the reversible or equilibrium equations of motion due to not allowing for either external heat or work sources. The molecular dynamic method, while tracking each particle, is still considered a statistical method since both spatial and temporal averages must be taken to extract any useful information from the simulations.

Appendix C Direct Simulation Monte Carlo (DSMC)

The DSMC method is an alternative computer simulation technique that tracks individual particles similar to the molecular dynamic method. The theoretical model behind the DSMC method is the Boltzmann equation. The main difference between the DSMC method and the MD method is that the DSMC takes a probabilistic approach to the intermolecular collisions [12, 13] while the MD method takes a deterministic approach [54]. Put another way, the DSMC method must always have a particle number less than the actual number of particles in the system to obtain a sufficient statistical average and the MD method will have a particle number equal to the true number of particles in the system. This illustrates the main benefit of using the DSMC, which is the reduced complexity of the simulation yielding faster run times.

Appendix D Burnett Hydrodynamics

The Burnett hydrodynamic equations (3.1), (3.2) and (3.3) are known to violate a number of thermodynamic and mechanical principles [11, 15]. The most notable are: violation of the second law of thermodynamics at higher Knudsen numbers [56] and mechanical instabilities under small wave length perturbations [15, 57]. Another issue with this set of equations is that the convergence properties are still generally unknown [15]. These difficulties have led to many attempts to rectify the problems. We will list a few of the more notable ones below:

In 1991, Zhong [16] added linearized third order terms to stabilize the Burnett equations. However, these augmented equations were not entirely successful at modeling blunt body wakes and flat plate boundary layers. However, Welder et al [58] showed that due to the nonlinear terms in the Burnett equations, a linear stability analysis alone is insufficient to explain to instabilities at higher Knudsen numbers.

1996-1997, Balakrishnan and Agarwal [17] simplified the nonlinear collision integral and replaced the material derivative terms with spatial derivatives from the Navier-Stokes equations, which has been said to have no physical basis [15]. These simplifications solved many of the problems and is known as the BGK-Burnett equations.

Appendix E MATLAB Code for Numerical Solutions

```
function Bivelocity_Numerical_Solver
clear all; clc; close all;
global uMax; %upper plate velocity
global Kn; %Knudsen Number

gamma=5/3; %specific heat ratio for the gas
Kn_Calc=[0.01 0.16 0.39 0.78];%Set of Kn numbers used for analysis

%Defining the figures that will be used for plotting the results
figure(1); hold on; hFig1 = figure(1);
figure(2); hold on; hFig2 = figure(2);
figure(3); hold on; hFig3 = figure(3);
figure(4); hold on; hFig4 = figure(4);

Mach=3; %Mach number of upper plate. Defined as u/c

%regardless of the knudsen numbers that I want to calculate the solution
%for, I will always calculate the knudsen=0 case first and use this
%solution as my initial guess for the finite knudsen cases

uMax=gamma^0.5*Mach; %Multiplied by gamma^0.5 because of non-dimensional

linestylelist={'-';':';'--';'-.'}; %A list of linestyles used

j=1;
%j=1 is the Burnett equations (burnett)
%j=2 is the bivelocity equations
Kn=0; %starting with Kn=0 to form guess structure
Max_Mesh=1000; %setting the mesh resolution

%initial guess structure for ODE solver
solinit=bvpinit(linspace(0,1,Max_Mesh),[1 1 1 1]);

options=bvpset('RelTol',1e-5,'NMax',Max_Mesh); %sets the solution options
%and max number of grid points to speed up calculations
if j==1

%bvp4c(ODE function, boundary)
```

```
sol = bvp4c(@Burnett,@ex2bc,solinit,options);
else
sol = bvp4c(@Fullequations,@ex2bc,solinit,options)
end

%conditions function, initial guess, options)
yguess(:,1) = sol.y(1,:); %velocity
yguess(:,2) = sol.y(2,:); %velocity derivative
yguess(:,3) = sol.y(3,:); %Temperature
yguess(:,4) = sol.y(4,:); %Temperature derivative
yguess(:,5) = 1./sol.y(3,:); %density
yguess(:,6) = -sol.y(4,:)./sol.y(3,:).^2; %density derivative
finite_kn_guess=guess(sol.x,yguess); %guess structure
%now have the solution for a knudsen=0 and can use this as an initial guess

for i=1:length(Kn_Calc)

    %Now solving the full set of equations
    Kn=Kn_Calc(i);
    if j==1
        sol = bvp4c(@Burnett,@ex2bc,finite_kn_guess,options);
    else
        sol = bvp4c(@Fullequations,@ex2bc,finite_kn_guess,options);
    end

    %up=u' ; Tp=T'; rhop = rho'
    u=sol.y(1,:); up=sol.y(2,:);
    T=sol.y(3,:); Tp=sol.y(4,:);
    rho=sol.y(5,:); rhop=sol.y(6,:);
    jv=3/2*T./rho.^2.*rhop;

    %plotting the pressure
    figure(1)
    plot(rho.*T,sol.x,strcat(linestylelist{i},'k'),'LineWidth',1.5)

    %plotting the temperature
    figure(2)
    plot(T,sol.x,strcat(linestylelist{i},'k'),'LineWidth',1.5)

    %plotting the volume flux (only if bivelocity)
    if j==2
        figure(3)
        plot(jv,sol.x,strcat(linestylelist{i},'k'),'LineWidth',1.5)
    end
```

```
    %plotting the density
    figure(4)
    plot(rho,sol.x,strcat(linestylelist{i},'k'),'LineWidth',1.5)

end

%setting up the legend
for k=1:length(Kn_Calc)
s{k} = sprintf('Kn_0 = %.2f', Kn_Calc(k));
end
s{k+1} = 'Velocity';

figure(1)
%pressure plot
box on %put the box around the plot
legend(s) %outputting the legend
ylabel('$y/H$','interpreter','latex', 'FontSize', 15,'rot',90)
% xlabel('$\tilde u,\tilde T$','interpreter','latex', 'FontSize', 20)
xlabel('$\tilde p$','interpreter','latex', 'FontSize', 20)
ylabh = get(gca,'YLabel');
set(ylabh,'Position',get(ylabh,'Position') - [0 0 0])
xlim([0.9 3])
set(hFig1, 'Position', [100 100 889 500])
%Printing the Figure to eps format for quality importing into Latex
set(gcf, 'PaperPositionMode', 'auto');
print -depsc2 Pressure.eps

figure(3)
%volume flux, only for bivelocity
box on
% plot(u,sol.x,strcat('*','k'),'MarkerSize',4)
legend(s,'Location','best')
ylabel('$y/H$','interpreter','latex', 'FontSize', 15,'rot',90)
%xlabel('$\tilde u,\tilde T$','interpreter','latex', 'FontSize', 20)
xlabel('$\tilde j_v$','interpreter','latex', 'FontSize', 20)
ylabh = get(gca,'YLabel');
set(ylabh,'Position',get(ylabh,'Position') - [0 0 0])
%xlim([-4 4])
set(hFig3, 'Position', [100 100 889 500])
%Printing the Figure to eps format for quality importing into Latex
set(gcf, 'PaperPositionMode', 'auto');
print -depsc2 flux.eps

figure(4)
%density
```

```
box on
% plot(u,sol.x,strcat('*','k'),'MarkerSize',4)
legend(s)
ylabel('$y/H$','interpreter','latex', 'FontSize', 15,'rot',90)
%xlabel('$\tilde u,\tilde T$','interpreter','latex', 'FontSize', 20)
xlabel('$\tilde \rho$','interpreter','latex', 'FontSize', 20)
ylabh = get(gca,'YLabel');
set(ylabh,'Position',get(ylabh,'Position') - [0 0 0])
if j==1
else
    xlim([0.6 1.1])
end

set(hFig4, 'Position', [100 100 889 500])
%Printing the Figure to eps format for quality importing into Latex
set(gcf, 'PaperPositionMode', 'auto');
print -depsc2 Density.eps

figure(2)
%Temp and velocity plot
box on
plot(u,sol.x,'k','LineWidth',1)
if j==1
    s='';
    s{1}='Velocity'
    s{2}='Temperature'
end

legend(s)
set(hFig2, 'Position', [100 100 889 500])
ylabel('$y/H$','interpreter','latex', 'FontSize', 15,'rot',90)
xlabel('$\tilde u,\tilde T$','interpreter','latex', 'FontSize', 20)
ylabh = get(gca,'YLabel');
set(ylabh,'Position',get(ylabh,'Position') - [0 0 0])
set(gcf, 'PaperPositionMode', 'auto');
print -depsc2 Velocity.eps

function dydx = Fullequations(~,y) %Bivelocity
%y(1)=u   | %y(3)=T   | %y(5)=rho
%y(2)=u'  | %y(4)=T'  | %y(6)=rho'
global Kn;
y1=y(1);y2=y(2);y3=y(3);y4=y(4);
if Kn==0
    dydx=[y2 %u'
        -1/y3*y4*y2 %u''
```

```
        y4 %T'
        -1/y3*y4^2-4/15*y2^2]; %T''
else
    y5=y(5);y6=y(6);
    dydx=[y2 %u'
        -1/y3*y4*y2 %u''
        y4 %T'
        -1/y3*y4^2-4/9*y2^2-1/3*1/y3^2*(1-y5*y3)/(Kn^2) %T''
        y6
        y5^2/y3^2*(y5*y3 - 1)/(2*Kn^2) - 1/y3*y6*y4 + 2/y5*y6^2];
end

function dydxBurnett = Burnett(~,y) %Bivelocity
%y(1)=u   | %y(3)=T   | %y(5)=rho
%y(2)=u'  | %y(4)=T'  | %y(6)=rho'
global Kn;
y1=y(1);y2=y(2);y3=y(3);y4=y(4);
if Kn==0
    dydxBurnett=[y2 %u'
        -1/y3*y4*y2 %u''
        y4 %T'
        -1/y3*y4^2-4/15*y2^2]; %T''
else
    y5=y(5);y6=y(6);
    dydxBurnett=[y2 %u'
        -1/y3*y4*y2 %u''
        y4 %T'
        -1/y3*y4^2-4/15*y2^2 %T''
        y6
        3/4*y5^2/y3^2*(y5*y3-1)/(Kn^2)-19/30*y5/y3*y2^2...
        +y5/y3^2*y4^2+1/y5*y6^2-1/y3*y6*y4];
end

%boundary condition function that uses one of two equations depending on
%whether or not the knudsen number is equal to zero
function res = ex2bc(ya,yb)
global uMax;
global Kn;
if Kn==0
    res=[ya(1)
     yb(1) - uMax %change this value to change upper plate velocity
     ya(3) - 1  %unity temp deriv at bottom
     yb(3) - 1]; %Temp is equal to one on upper plate
else
    res=[ya(1)
```

```
     yb(1) - uMax% + Kn*sqrt(pi/2)*yb(2)
     ya(3) - 1  %unity temp deriv at bottom
     yb(3) - 1 %Temp is equal to one on upper plate
     ya(5) - 1
     yb(5) - 1];
end

%structure used to form the intial guess for the finite knudsen case.
%I use the zero knudsen case as the initial guess
function solguess = guess(x,y)
    solguess.x = x;
    solguess.y = y';
```

References

[1] CM Ho and YC Tai. Micro-electro-mechanical-systems (MEMS) and fluid flows. *ANNUAL REVIEW OF FLUID MECHANICS*, 30:579–612, 1998.

[2] Howard Brenner. Proposal of a critical test of the navier-stokes-fourier paradigm for compressible fluid continua. *Phys. Rev. E*, 87(1):013014, January 2013.

[3] Ching Shen. *Rarefied gas dynamics: fundamentals, simulations and micro flows*. Springer, 2005.

[4] Mohamed Gad-el Hak. The fluid mechanics of microdevices-the freeman scholar lecture. *TRANSACTIONS-AMERICAN SOCIETY OF MECHANICAL ENGINEERS JOURNAL OF FLUIDS ENGINEERING*, 121:533, 1999.

[5] Martin Knudsen. The law of the molecular flow and viscosity of gases moving through tubes. *Ann. Phys*, 28:75130, 1909.

[6] W. Steckelmacher. Knudsen flow 75 years on: the current state of the art for flow of rarefied gases in tubes and systems. *Reports on Progress in Physics*, 49(10):1083, 1986.

[7] LD Landau. Fluid mechanics: Volume 6 (course of theoretical physics) author: LD landau, EM lifshitz, publisher: Bu. 1987.

[8] R Byron Bird, Warren E Stewart, and Edwin N Lightfoot. Transport phenomena. 1960. *Madison, USA*, 1960.

[9] SR de Groot and P Mazur. Non-equilibrium thermodynamics. 1962.

[10] Sydney Chapman and Thomas George Cowling. *The mathematical theory of non-uniform gases: an account of the kinetic theory of viscosity, thermal conduction and diffusion in gases*. Cambridge university press, 1991.

[11] Ramesh K. Agarwal, Keon-Young Yun, and Ramesh Balakrishnan. Beyond NavierStokes: burnett equations for flows in the continuumtransition regime. *Physics of Fluids*, 13(10):3061–3085, 2001.

[12] GA Bird. Approach to translational equilibrium in a rigid sphere gas. *Physics of Fluids*, 6:1518, 1963.

[13] GA Bird. Monte carlo simulation of gas flows. *Annual Review of Fluid Mechanics*, 10(1):1131, 1978.

[14] D Burnett. The distribution of velocities in a slightly non-uniform gas. *Proceedings of the London Mathematical Society*, 2(1):385430, 1935.

[15] S. Kokou Dadzie. A thermo-mechanically consistent burnett regime continuum flow equation without ChapmanEnskog expansion. *Journal of Fluid Mechanics*, 716, 2013.

[16] Xiaolin Zhong. *Development and computation of continuum higher order constitutive relations for high-altitude hypersonic flow*. Stanford University, 1991.

[17] Ramesh Balakrishnan and Ramesh Agarwal. Entropy consistent formulation and numerical simulation of the BGK-Burnett equations using a kinetic wave/particle flux splitting algorithm. In Paul Kutler, Jolen Flores, and Jean-Jacques Chattot, editors, *Fifteenth International Conference on Numerical Methods in Fluid Dynamics*, volume 490 of *Lecture Notes in Physics*, pages 480–485. Springer Berlin / Heidelberg, 1997. 10.1007/BFb0107148.

[18] Howard Brenner. Is the tracer velocity of a fluid continuum equal to its mass velocity? *Phys. Rev. E*, 70(6):061201, December 2004.

[19] Howard Brenner. Navier-stokes revisited. *Physica A: Statistical Mechanics and its Applications*, 349(1-2):60 – 132, 2005.

[20] Howard Brenner. Bi-velocity hydrodynamics. *Physica A: Statistical Mechanics and its Applications*, 388(17):3391 – 3398, 2009.

[21] Howard Brenner. Beyond NavierStokes. *International Journal of Engineering Science*, 54(0):67 – 98, 2012.

[22] Howard Brenner and James R. Bielenberg. A continuum approach to phoretic motions: Thermophoresis. *Physica A: Statistical Mechanics and its Applications*, 355(24):251 – 273, 2005.

[23] S. Kokou Dadzie and Howard Brenner. Predicting enhanced mass flow rates in gas microchannels using nonkinetic models. *Phys. Rev. E*, 86(3):036318, September 2012.

[24] CHRISTOPHER J. GREENSHIELDS and JASON M. REESE. The structure of shock waves as a test of brenner's modifications to the NavierStokes equations. *Journal of Fluid Mechanics*, 580:407429, 2007.

[25] John Tyndall. *On dust and disease*. W. Clowes and Sons, 1870.

[26] John Aitken. XV.On the formation of small clear spaces in dusty air. *Transactions of the Royal Society of Edinburgh*, 32(02):239272, 1884.

[27] S. Kokou Dadzie, Jason M. Reese, and Colin R. McInnes. A continuum model of gas flows with localized density variations. *Physica A: Statistical Mechanics and its Applications*, 387(24):6079 – 6094, 2008.

[28] S. Kokou Dadzie and Jason M. Reese. Analysis of the thermomechanical inconsistency of some extended hydrodynamic models at high knudsen number. *Phys. Rev. E*, 85(4):041202, April 2012.

[29] Leonhard Euler. Principes generaux du movement des fluides. *Abhandlungen der Kniglichen Akademie der Wissenschaften zu Berlin*, 1757.

[30] Peter Kostdt and Mario Liu. Three ignored densities, frame-independent thermodynamics, and broken galilean symmetry. *Phys. Rev. E*, 58(5):55355540, November 1998.

[31] Mario Liu. Comment on Weakly and strongly consistent formulations of irreversible processes. *Phys. Rev. Lett.*, 100(9):098901, March 2008.

[32] Hans Christian Öttinger. Öttinger replies:. *Phys. Rev. Lett.*, 100(9):098902, March 2008.

[33] Hans Christian Öttinger, Henning Struchtrup, and Mario Liu. Inconsistency of a dissipative contribution to the mass flux in hydrodynamics. *Phys. Rev. E*, 80(5):056303, November 2009.

[34] Howard Brenner. Fluid mechanics in fluids at rest. *Phys. Rev. E*, 86(1):016307, July 2012.

[35] Howard Brenner. Kinematics of volume transport. *Physica A: Statistical Mechanics and its Applications*, 349(12):11 – 59, 2005.

[36] Byung Chan Eu. Volume transport and generalized hydrodynamic equations for monatomic fluids. *The Journal of Chemical Physics*, 129(13):134509, 2008.

[37] Byung Chan Eu. Molecular theory of barycentric velocity: Monatomic fluids. *The Journal of Chemical Physics*, 128(20):204507, 2008.

[38] Byung Chan Eu. Molecular representation of molar domain (volume), evolution equations, and linear constitutive relations for volume transport. *The Journal of Chemical Physics*, 129(9):094502, 2008.

[39] Jagtar Singh Hunjan and Byung Chan Eu. The voronoi volume and molecular representation of molar volume: Equilibrium simple fluids. *The Journal of Chemical Physics*, 132(13):134510, 2010.

[40] J. Clerk Maxwell. On stresses in rarified gases arising from inequalities of temperature. *Philosophical Transactions of the Royal Society of London*, 170:231–256, 1879.

[41] Howard Brenner. Beyond the no-slip boundary condition. *Phys. Rev. E*, 84(4):046309, October 2011.

[42] G. G. Stokes. On the theories of the internal friction of fluids in motion, and of the equilibrium and motion of elastic solids. *Transactions of the Cambridge Philosophical Society*, VIII(Part III):287–319, April 1845.

[43] G. G. Stokes. On the dynamical theory of diffraction. *Transactions of the Cambridge Philosophical Society*, 9:1–62, November 1849.

[44] Nishanth Dongari, Franz Durst, and Suman Chakraborty. Predicting microscale gas flows and rarefaction effects through extended Navier-StokesFourier equations from phoretic transport considerations. *Microfluidics and Nanofluidics*, 9(4-5):831–846, 2010.

[45] Nishanth Dongari, Ashutosh Sharma, and Franz Durst. Pressure-driven diffusive gas flows in micro-channels: from the knudsen to the continuum regimes. *Microfluidics and Nanofluidics*, 6(5):679–692, 2009.

[46] Nishanth DONGARI, Rajamani SAMBASIVAM, and Franz DURST. Extended navier-stokes equations and treatments of micro-channel gas flows. *Journal of Fluid Science and Technology*, 4(2):454–467, 2009.

[47] Suman Chakraborty and Franz Durst. Derivations of extended navier-stokes equations from upscaled molecular transport considerations for compressible ideal gas flows: Towards extended constitutive forms. *Physics of Fluids*, 19(8):088104, 2007.

[48] Paul S Epstein. Zur theorie des radiometers. *Zeitschrift fr Physik A Hadrons and Nuclei*, 54(7):537563, 1929.

[49] Duncan A. Lockerby and Jason M. Reese. High-resolution burnett simulations of micro couette flow and heat transfer. *Journal of Computational Physics*, 188(2):333 – 347, 2003.

[50] H. Xue, H. M. Ji, and C. Shu. Analysis of micro-couette flow using the burnett equations. *International Journal of Heat and Mass Transfer*, 44(21):4139 – 4146, 2001.

[51] Vicente Garz and Andrs Santos. *Kinetic theory of gases in shear flows: nonlinear transport*, volume 131. Springer, 2003.

[52] C. J. Lee. Unique determination of solutions to the burnett equations. *AIAA Journal*, 32(5):985–990, May 1994.

[53] Lawrence F Shampine, Jacek Kierzenka, and Mark W Reichelt. Solving boundary value problems for ordinary differential equations in MATLAB with bvp4c. *Tutorial Notes*, 2000.

[54] W G Hoover. Nonequilibrium molecular dynamics. *Annual Review of Physical Chemistry*, 34(1):103–127, 1983.

[55] Leopold Alexander Pars. *A treatise on analytical dynamics*, volume 86. Heinemann London, 1965.

[56] Keith Comeaux, Dean Chapman, Ma, and Robert Cormack. An analysis of the burnett equations based on the second law of thermodynamics. In *33rd Aerospace Sciences Meeting and Exhibit*, Aerospace Sciences Meetings. American Institute of Aeronautics and Astronautics, January 1995.

[57] KURTA FISCKO and DEANR CHAPMAN. Comparison of burnett, super-burnett and monte carlo solutions for hypersonic shock structure. *Rarefied gas dynamics: Theoretical and computational techniques*, page 374395, 1989.

[58] Wallace T Welder, Dean R Chapman, and Robert W MacCormack. Evaluation of various forms of the burnett equations. In *AIAA*, volume 1, 1993.